Biophysical and proteomic analyses suggest functions of *Pseudomonas syringae* pv *tomato* DC3000 extracellular vesicles in bacterial growth during plant infection

Martin Janda[1,2,+], Christina Ludwig[3], Katarzyna Rybak[1], Chen Meng[3], Egidio Stigliano[4,5], Leon Botzenhardt[1], Beata Szulc[1], Jan Sklenar[4], Frank L.H. Menke[4], Jacob G. Malone[5,6], Andreas Brachmann[1], Andreas Klingl[1] and Silke Robatzek[1#]

[1]LMU Biocenter, Ludwig-Maximilian-University of Munich, Großhaderner Strasse 4, 82152 Martinsried, DE

[2]University of Chemistry and Technology Prague, Department of Biochemistry and Microbiology, Technická 5, Prague 6 – Dejvice 166 28, CZ

[3]Bavarian Center for Biomolecular Mass Spectrometry (BayBioMS), Technical University of Munich, Gregor-Mendel-Strasse 4, 85354 Freising, DE

[4]The Sainsbury Laboratory, Norwich Research Park, NR4 7UH, UK

[5]John Innes Centre, Norwich Research Park, NR4 7UH, UK

[6]University of East Anglia, Norwich Research Park, NR4 7TJ, UK

[+]Present address: Faculty of Science, University of South Bohemia in České Budějovice, Branišovská 1645/31a, České Budějovice, CZ

[#]Correspondence: Silke Robatzek

LMU Biocenter

Tel.: +49-2180-74124

Email: robatzek@bio.lmu.de

Short title: Analysis of *Pto* DC3000 extracellular vesicles

Key words: Extracellular vesicles, EVs, *Pto* DC3000, proteomics, pattern-triggered immunity, PTI, nanoparticle tracking analysis, NTA, *Arabidopsis thaliana*

Manuscript information: Summary (180 words), text excluding references (10.450 words). The number of figures: 8 main figures; 6 supplemental figures; 2 main tables; 6 supplemental tables.

Summary

Vesiculation is a process employed by Gram-negative bacteria to release extracellular vesicles (EVs) into the environment. Bacterial EVs contain molecular cargo from the donor bacterium and play important roles in bacterial survival and growth. Here, we describe EV production in plant-pathogenic *Pseudomonas syringae* pv. *tomato* DC3000 (*Pto* DC3000), the causal agent of bacterial speck disease. Cultured *Pto* DC3000 exhibited EV structures both on the cell surface and in the vicinity of bacterial cells, observed as outer membrane vesicle (OMV) release. We used in-solution trypsin digestion coupled to mass spectrometry to identify 369 proteins enriched in EVs recovered from cultured *Pto* DC3000. The predicted localization profile of EV proteins supports the production of EVs also in the form of outer-inner-membrane vesicles (OIMVs). EV production varied slightly between bacterial lifestyles and also occurred *in planta*. The potential contribution of EVs to *Pto* DC3000 plant infection was assessed using plant treatments and bioinformatic analysis of the EV-enriched proteins. While these results identify immunogenic activities of the EVs, they also point at roles for EVs in bacterial defences and nutrient acquisition by *Pto* DC3000.

Introduction

Successful colonization of hosts depends on the ability of microbes to defend themselves against host immune responses and acquire nutrients. Bacterial pathogens use macromolecular translocation systems and deliver virulence proteins, so-called effectors, to circumvent host immunity (Buttner & Bonas, 2010). *Pseudomonas syringae* pv. *tomato* (*Pto*) DC3000 is the causal agent of bacterial speck, a common disease that occurs in tomato production worldwide (Mansfield *et al.*, 2012, Wilson *et al.*, 2002). *Pto* DC3000 is a Gram-negative bacterium that invades through openings in the plant surface and propagates in the apoplast, where it takes up nutrients and proliferates (Melotto *et al.*, 2006, Xin & He, 2013, Xin *et al.*, 2018). Plants

respond rapidly to colonization by microbes, activating innate defence strategies, which can broadly be categorized into pattern-triggered immunity (PTI) activated by microbe-associated molecular patterns (MAMPs) and effector-triggered immunity (ETI) induced upon recognition of virulence factors or their actions (Couto D. & Zipfel, 2016, Dodds & Rathjen, 2010). Virulence of *Pto* DC3000 largely depends on the Type-III secretion system and its secreted effectors (Kvitko *et al.*, 2009, Nobori *et al.*, 2018, Nobori *et al.*, 2019, Nomura *et al.*, 2006). A number of Type-III secreted effectors from *Pto* DC3000 and their *in planta* targets have been identified, many involved in immune suppression and some with roles in gaining access to nutrients (Wei *et al.*, 2018, Xin *et al.*, 2018). For example, genes encoding proteins for siderophore biosynthesis are upregulated *in planta* (Nobori *et al.*, 2018). In addition, pathogenic bacteria need to adapt to the host environment, resisting the defences induced by the host immune system.

The survival of infectious Gram-negative bacteria is greatly enhanced by releasing extracellular vesicles (EVs), a process widely studied in the context of bacteria pathogenic to humans (Schwechheimer & Kuehn, 2015). During infection, bacterial EVs can counteract the effect of antimicrobial peptides (Roszkowiak *et al.*, 2019). They also perform immunomodulatory functions by delivering virulence factors to recipient cells resulting in immune-suppression (Kaparakis-Liaskos & Ferrero, 2015), despite having the capacity to activate defences due to their immunogenic cargoes (Kaparakis-Liaskos & Ferrero, 2015). More recently, a number of studies provide evidence that plant pathogenic bacteria, including cultured *Pto* bacteria release EVs (Bahar *et al.*, 2016, Chowdhury & Jagannadham, 2013, McMillan *et al.*, 2020). Although insights into both immunogenic and virulent roles have been achieved, little is currently known about the importance of EV production in bacterial infection success.

EVs are cytosol-containing membrane "nano" spheres that provide selection, storage and protection against degradation of enclosed cargoes in a highly dynamic and environmental cue-responsive manner (Bielska *et al.*, 2019, Rybak & Robatzek, 2019, Schwechheimer & Kuehn, 2015). Gram-negative bacteria actively form EVs by budding and shedding of the outer membrane, producing so-called outer membrane vesicles (OMVs) (Raposo & Stoorvogel, 2013, Roier *et al.*, 2016). Outer-inner-membrane vesicles (OIMVs) have also been described, involving a different mode of release such as endolysin-triggered cell lysis (Perez-Cruz *et al.*, 2015, Toyofuku *et al.*, 2019). EVs can also be produced in the form of elongated, tube-shaped vesicles as observed in Gram-negative *Francisella* spp. (McCaig *et al.*, 2013, Sampath *et al.*, 2018). As insufficient biomarkers are available to convincingly probe their origin, in particular for *P. syringae*, we will collectively refer to these vesicles as EVs. Notably, EV formation seems to be an essential process since no bacterial mutant lacking vesicle release has been reported so far and genetic reduction of vesiculation results in mutants with growth defects (McBroom *et al.*, 2006).

Previous studies revealed a number of molecular cargoes present in EVs from phytopathogenic bacteria of the *Agrobacterium tumefaciens*, *P. syringae*, *Xanthomonas campestris* and *Xylella fastidiosa* species. These EV-associated proteins include degradative enzymes, Type-II-secreted virulence-associated proteins, components of the Type-III secretion system and its secreted proteins (Feitosa-Junior *et al.*, 2019, Chowdhury & Jagannadham, 2013, Knoke *et al.*, 2020, Nascimento *et al.*, 2016, Sidhu *et al.*, 2008, Sole *et al.*, 2015). While respective genetic deletions of EV-associated degradative enzymes reduced bacterial virulence, the role of EVs in their delivery remained unanswered (Nascimento *et al.*, 2016, Sidhu *et al.*, 2008, Sole *et al.*, 2015). A previous seminal study described the production of EVs as a mechanism, by which *X. fastidiosa* regulates its attachment to host cells and thus the promotes systemic infection

(Ionescu *et al.*, 2014). However, elongation factor Tu (EF-Tu) and lipopolysaccharides (LPS) are abundant components of EVs from *P. syringae*, *X. campestris*, *X. oryzae* and *X. fastidiosa* (Bahar *et al.*, 2016, Feitosa-Junior *et al.*, 2019, Chowdhury & Jagannadham, 2013, Sidhu *et al.*, 2008). Both represent MAMPs, with EV-associated EF-Tu shown to activate a prototypic PTI response in a receptor-dependent manner (Bahar *et al.*, 2016). Further results indicate that EV-induced immunity, triggered with EVs recovered from pathogenic *Pto* DC3000 and the commensal *P. fluorescens*, protects plants against *Pto* DC3000 infection (McMillan *et al.*, 2020). These studies hint at some contrasting roles that EVs from bacterial phytopathogens could play during plant infection.

Here, we used nanoparticle tracking analysis (NTA) to describe the production and the biophysical properties of EVs from *Pto* DC3000 in different growth conditions including their accumulation *in planta*. Analysis of *Pto* DC3000 cellular, outer membrane (OM) and EV proteomes by mass spectrometry identified 369 EV-enriched proteins. The potential contribution to bacterial growth *in planta* of these proteins was assessed using bioinformatic analysis as well as exploring plant responses to EVs. These findings expand our understanding of the functions of EVs in bacterial infection of plants.

Results

Pto DC3000 bacteria vesiculate and produce EVs in culture

We first examined the morphology of *Pto* DC3000 cultures by scanning electron microscopy (SEM). The bacteria displayed multiple spherical structures protruding from their cell surfaces, with diameters in the range of 20-120 nm (Fig. 1A; S1A). These vesicle-like structures appeared to be released from the surface, as similarly sized vesicular structures could also be observed in the vicinity of the bacteria (Fig. S1A). To determine whether these structures were released

133 from the bacterial cell surface, supernatants of planktonic *Pto* DC3000 cultures were filtered
134 through 0.22µm-pore membranes to remove intact bacteria and measured by Nanoparticle
135 Tracking Analysis (NTA) before (fluid sample) and after sucrose density gradient
136 centrifugation followed by ultracentrifugation (gradient-enriched sample) (Fig. S2A). Density
137 gradient centrifugation is used to separate EVs from other extracellular materials (Klimentova
138 & Stulik, 2015). NTA measures particle number (concentration), particle size (median diameter
139 and distribution), and particle surface charge (mean ζ-potential). Both sample types exhibited a
140 polydisperse sized population of spherical structures with a diameter ranging from ~ 50 to 200
141 nm and median sizes of 100 nm and 115 nm for fluid samples and gradient enriched samples,
142 respectively (Fig. 1C, 1G, S1B). This could suggest that *Pto* DC3000 releases vesicles from
143 different biogenesis routes.
144
145 Pellets obtained from gradient enriched samples were further examined by SEM and revealed
146 numerous spherical structures (Fig. 1B), yet in this analysis the vesicles diameter ranged
147 between 25 and 170 nm with a median around 50 nm. It is possible that conditions used for
148 SEM and NTA differ in their capacity to hydrate the vesicles and/or that NTA underestimates
149 smaller particles (Bachurski *et al.*, 2019). In addition, co-purifying filamentous structures could
150 be detected (Fig. 1B). To determine whether EV production is an active process, EVs were
151 quantified from culture supernatants of *Pto* DC3000 over cultivation time, with increasing
152 particle numbers observed with bacterial density (Fig. 1D, 1E, S2B). While the total amount of
153 EVs recovered from bacteria at late exponential growth was higher compared with early growth
154 stages (Fig. 1D, 1E), calculation of the amount of EVs produced per bacteria showed that
155 numbers were similar between growth stages (Fig. 1E). The median diameter and ζ-potential of
156 EVs was comparable across growth stages (Fig. 1F, 1G, 1H).
157

158 Quantification of EVs from *Pto* DC3000 cultures that were incubated in fresh media followed
159 by heat inactivation showed increased vesicle numbers (Fig. 1D). This suggests that heat
160 inactivation could additionally trigger the production of vesicles, i.e. from cellular debris and/or
161 through a process described as explosive cell lysis (Toyofuku *et al.*, 2019). Given this increase
162 and the distinct size of the vesicles from heat inactivated bacterial cultures (Fig. 1F), it suggests
163 that the vesicles recovered from culture samples without heat inactivation are predominantly
164 produced from bacteria as an active process.
165
166 EVs were also isolated from biofilm grown *Pto* DC3000 cultures (Fig. S2C, S2D). The median
167 diameter of these EVs was smaller compared with EVs from planktonic gradient enriched *Pto*
168 DC3000 EVs but had a similar size to EVs from fluid samples (Fig. 1G). The mean ζ-potential
169 of EVs from biofilm samples was similar to EVs from planktonic gradient enriched samples
170 but more negative than EVs from fluid samples of planktonic *Pto* DC3000 cultures (Fig. 1H).
171 Thus, EVs show diverse biophysical properties depending on bacterial lifestyle, further refuting
172 the possibility that the purified particles are solely formed through nonspecific assembly of shed
173 membrane fragments.
174

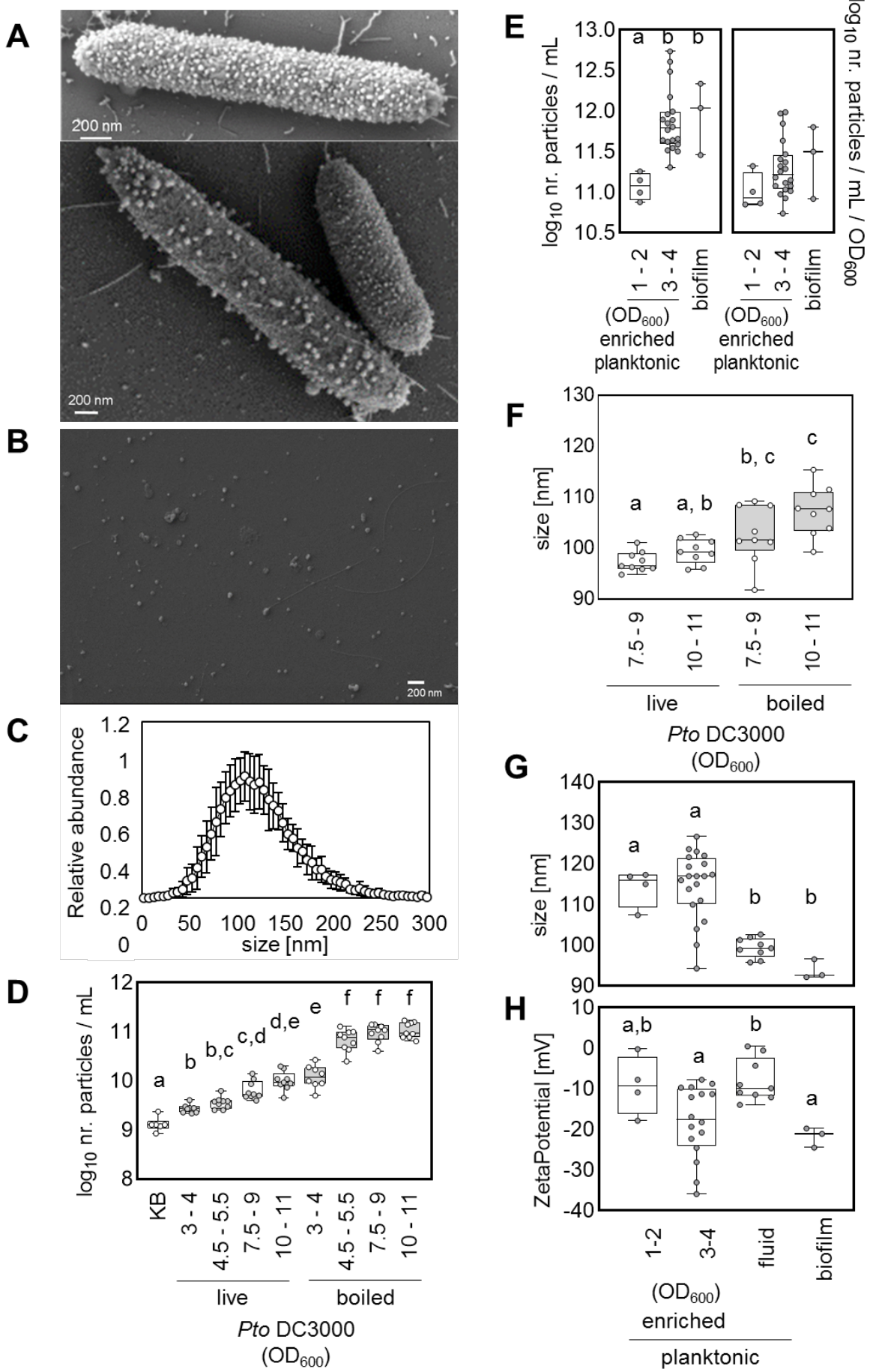

Figure 1. *Pto* DC3000 release extracellular vesicles with differing biophysical parameters depending on lifestyle. A) Representative SEM micrographs of *Pto* DC3000 growth in planktonic culture (OD_{600} = 3-4). **B)** Representative SEM micrograph of gradient enriched *Pto* DC3000 EVs purified from planktonic culture (OD_{600} = 3-4); scale bars represent 200 nm. For A and B, the micrographs were selected as representatives from three independent samples. For D-H each dot in the boxplot represents an independent sample. **C)** Size profile of gradient enriched EVs from *Pto* DC3000 planktonic cultures (OD_{600} = 3-4), the values represent mean and standard deviations from n = 20. Concentration **(D)** and size **(F)** of EVs from fluid samples before (live) and after heat inactivation of bacteria (boiled); King's B (KB) medium. Concentration **(E)**, size **(G)** and ζ-potential **(H)** of EVs from planktonic cultures (enriched = gradient enriched OD_{600} = 1-2 and 3-4 and fluid samples OD_{600} = 7.5 - 11) and of EVs from biofilm cultures. For D and F n = 8-9 independent samples, for samples in E and G n = 4 for OD_{600} = 1-2 and n = 20 for OD_{600} = 3-4 for gradient enriched samples, n = 9 for fluid samples and n=3 for biofilm. The box in boxplots extends from 25th to 75th percentiles, whiskers go down to the minimal value and up to the maximal value, the line in the middle of the box is plotted at the median. Different letters indicate significant (Welsch´s ANOVA with Dunnett´s T3 multiple comparisons post hoc test; $p < 0.05$).

To investigate whether the biophysical parameters of *Pto* DC3000 EVs could change upon mechanical treatments, we subjected the samples to sonication, heating and freezing. In addition, we tested the effect of incubation with Proteinase K, a treatment used to deplete the EV samples of extravesicular proteins (Metruccio *et al.*, 2016). None of the treatments significantly affected the particle concentration (Fig. 2). Also, particle size was not significantly changed upon sonication and Proteinase K treatments (Fig. 2A, 2D). A significant increase in particle size was observed after ten freeze-thaw cycles and longer heat exposure (Fig. 2B, 2C). These observations suggest that EVs are affected by more extreme temperature treatments, maybe forming higher aggregates, while sonication, shorter heat incubation, fewer freeze-thaw cycles and Proteinase K treatments showed no significant effects.

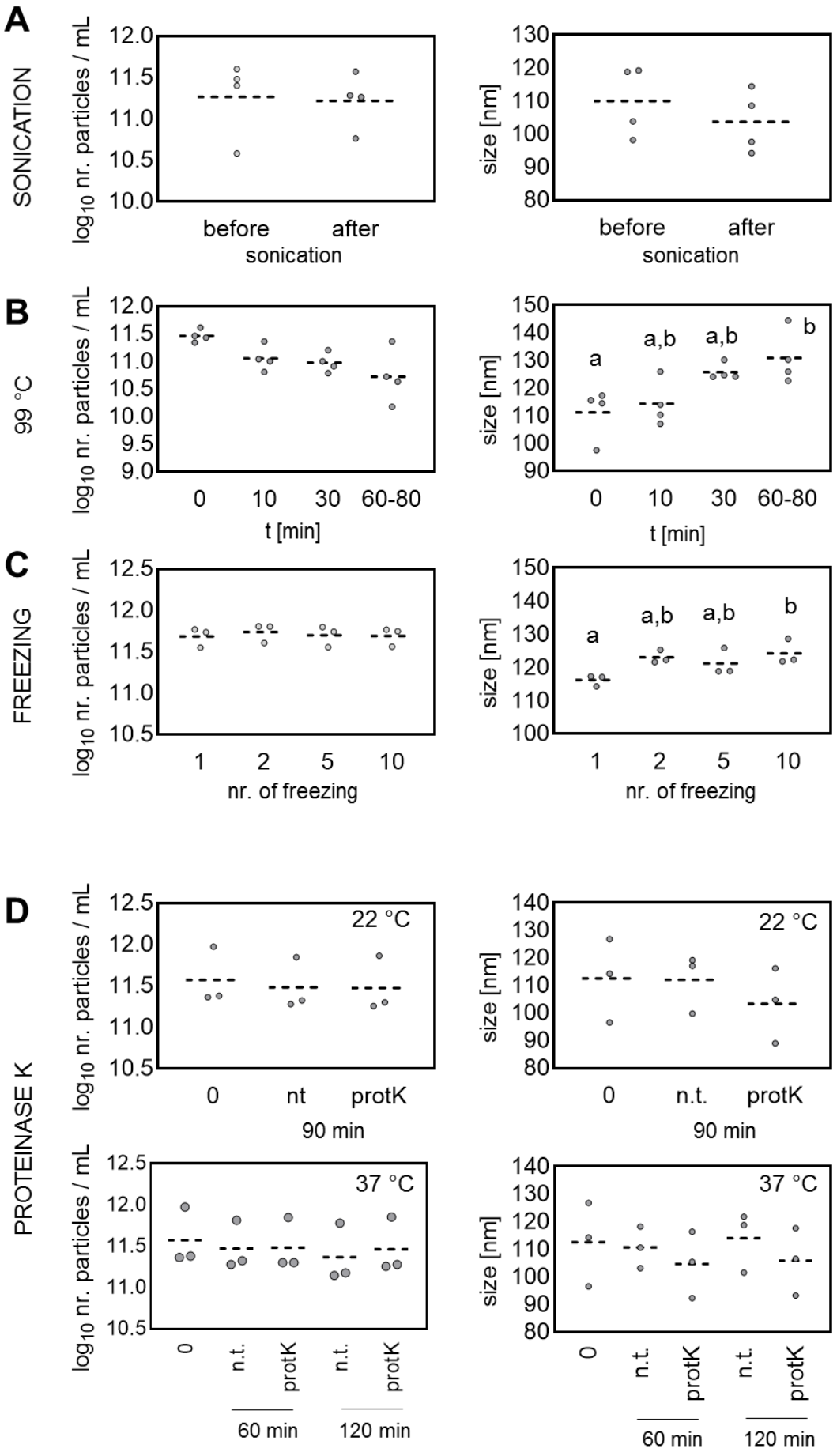

Figure 2. Disruptive treatments cause minor changes to biophysical parameters of gradient enriched EVs. Concentration and size analysis of *Pto* DC3000 EVs from planktonic cultures (OD_{600} = 3-4). Effects of **A)** sonication (10 times 30 s); **B)** 99 °C for 80 min; **C)** freezing and thawing (up to ten times); **D)** Proteinase K treatment (10 µg/mL) at 22 °C and 37 °C for up to 120 min. Individual circles represent particles characteristics from independent samples; n = 3 to 4. Different letters indicate significant difference (One-way ANOVA with Tukey post hoc test; $p < 0.05$).

187

188 ***Pto* DC3000 bacteria produce EVs *in planta***

189 To determine whether *Pto* DC3000 releases vesicles *in planta*, apoplastic fluids were recovered
190 from *Pto* DC3000-infected and control-treated *A. thaliana* leaf tissues at different time points.
191 The apoplastic fluids were collected, filtered to remove intact bacteria and then directly
192 characterized by NTA without density gradient centrifugation and ultracentrifugation. In these
193 apoplastic fluid samples, we identified particles with a median diameter of ~96 nm (Fig. 3A),
194 which increased in abundance upon infection with *Pto* DC3000 (Fig. 3B), consistent with
195 previous findings (Rutter & Innes, 2017). Increased particle abundance correlated with the
196 bacterial infection time and titers (Fig. 3B, Fig. S3A, S3B). We also analysed EVs from
197 apoplastic fluids of plants, which were co-treated with 100 nM flg22 and *Pto* DC3000. Particle
198 numbers were lower than those recovered from *Pto* DC3000 infection only, consistent with
199 induced plant defences (Fig. S3C). Taken together, the higher particle numbers and
200 polydisperse particle size isolated from *Pto* DC3000-infected plants compared to flg22
201 immune-stimulated plants hints at bacterial-derived EVs present in *A. thaliana* apoplastic fluids
202 (Fig. 3B).

203

204 Since *Pto* DC3000 (fluid sample) and *A. thaliana* (apoplastic fluid samples) EVs did not
205 significantly differ in diameter (Fig. 1G, 3A), we focused on the charge of EVs, reflecting the
206 different surface composition of bacterial (prokaryotic) and plant-derived (eukaryotic) EVs.
207 Evaluation of the mean ζ-potential identified significantly less negatively charged EVs
208 recovered from apoplastic fluids of *Pto* DC3000-infected plants at three days post infection

209 compared with control treatments and earlier time points (Fig. 3C, 3D, 3E, 3G). This time point
210 correlated with *in planta* bacterial proliferation and depended on bacterial inoculum (Fig. S3A,
211 S3B). Plotting the relative particle abundance over particle charge, the ζ-potential profiles of
212 EVs recovered from apoplastic fluids of untreated, control-treated and flg22-treated *A. thaliana*
213 identified major peaks around -32 mV (Fig. 3C, 3D, S3J). By contrast, the ζ-potential profile of
214 EVs recovered from apoplastic fluids of *Pto* DC3000-infected *A. thaliana* had a broader
215 distribution with a similar major peak around -32 mV and an additional shoulder around -10
216 mV (Fig. 3E, 3G). Comparison of the different ζ-potential profiles revealed similarities of the
217 major -32 mV peak across all plant samples, likely representing a plant-derived EV pool (Fig.
218 3C, 3D, S3J, S3K). Notably, the shoulder around -10 mV detected from apoplastic fluids of *Pto*
219 DC3000-infected plant samples showed large overlay with the ζ-potential profile of EV
220 recovered from *Pto* DC3000 cultures (fluid samples), with a peak from -20 to 0 mV (Fig. 3E,
221 3F, 3G). This could, therefore, represent a bacterial-derived EV pool. Since the ζ-potential
222 profiles of EVs recovered from apoplastic fluids of flg22-treated *A. thaliana* did not differ
223 between untreated or control-treated leaves (Fig. 3C, S3J, S3K), we found no evidence that
224 plant EVs modulate their surface charge during infection. Thus, our data strongly suggest that
225 *Pto* DC3000 release EVs during plant infection.
226

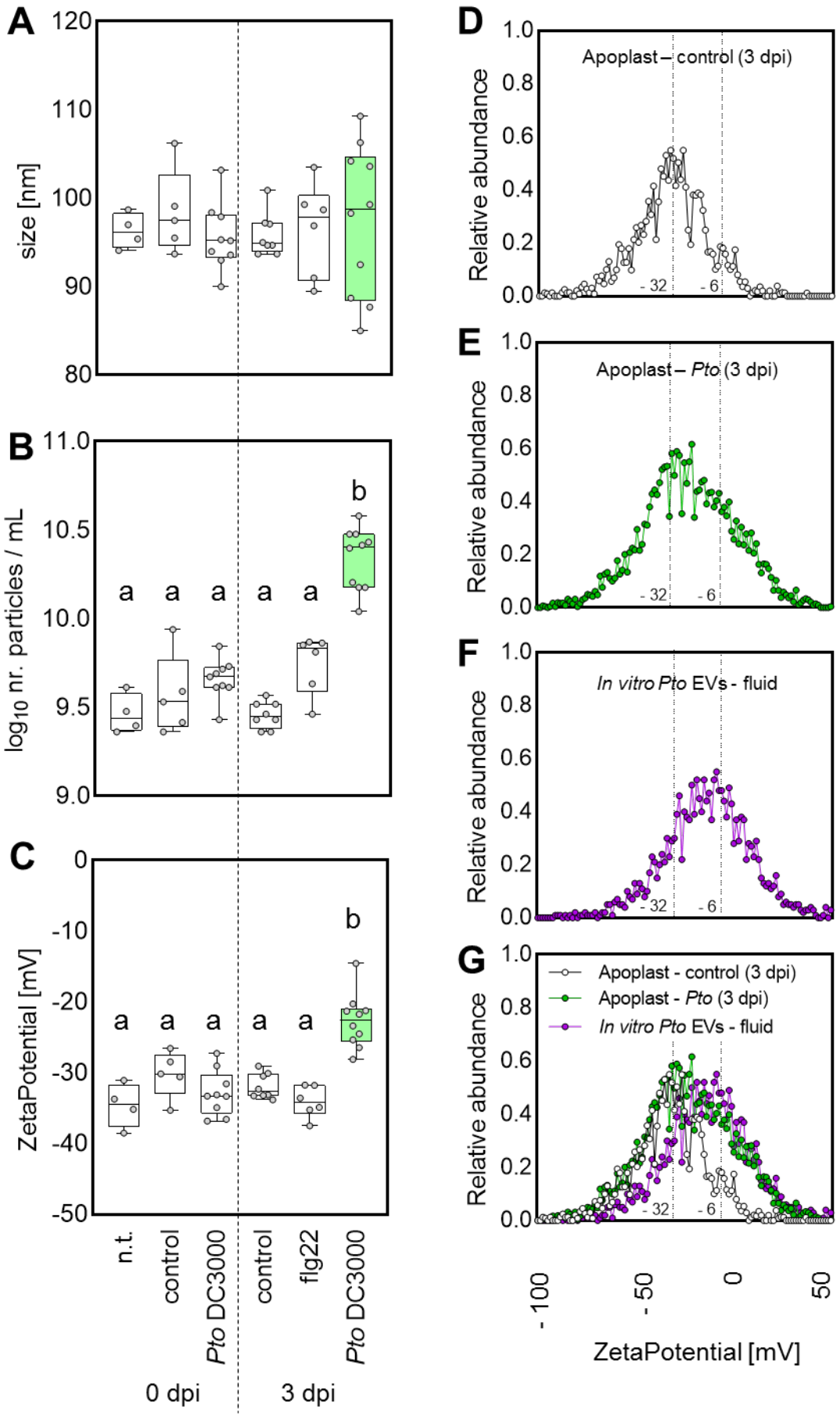

Figure 3. *Pto* DC3000 release EVs *in planta*. Size, concentration and charge measurements of apoplastic fluids from *A. thaliana* plants infected with *Pto* DC3000 and treated as indicated. **A)** Size of the particles. **B)** Particle concentration in apoplastic fluids. **C)** ζpotential of the particles. For A-C the variants represent: n.t. – non-treatment; control – 10 mM $MgCl_2$; *Pto* DC3000 (OD_{600} = 0.0006); 100 nM flg22. **D-G)** The profile of ζ-potential for particles detected in Arabidopsis apoplast treated with $MgCl_2$ (control; D) for 3 days, with *Pto* DC3000 (*Pto*; OD_{600} = 0.0006; E) for 3 days and for EVs from *Pto* DC3000 grown in culture (fluid; F). The dots represent the mean from 8 (D, G_white), 10 (E, G_green) and 13 (F, G_purple). For A-C each dot in the boxplot represents an independent sample. The box in boxplots extends from 25th to 75th percentiles, whiskers go down to the minimal value and up to the maximal value, the line in the middle of the box is plotted at the median. Different letters indicate significant difference (One-way ANOVA with Tukey post hoc test; $p < 0.05$). The green colour is highlighting the particles from *Pto* DC3000 infected plants (3 dpi).

EV samples purified from *Pto* DC3000 cultures trigger plant immune responses

Bacterial EVs contain immunogenic molecules such as EF-Tu and LPS, and can contain digestive enzymes and effectors that undermine host defences (Bahar *et al.*, 2016, Feitosa-Junior *et al.*, 2019, Knoke *et al.*, 2020, Rybak & Robatzek, 2019). To determine the effect of EVs from *Pto* DC3000 on plant cells, we first examined the ability of the *Pto* DC3000 EVs to modulate the outcome of bacterial infection. We pre-treated *A. thaliana* leaves with *Pto* DC3000 EVs, which limited the growth of subsequently infected *Pto* DC3000 bacteria *in planta* (Fig. 4A, S4A). Thus, the immunogenic potential of *Pto* DC3000 EVs is sufficient to restrict bacterial colonization, consistent with recent observations (McMillan *et al.*, 2020). Since MAMP treatment mediates anti-bacterial protection through the induction of plant immune reactions (Zipfel *et al.*, 2004), we next evaluated defence gene expression to EV treatment using *pFRK1*::GUS reporter lines (Kunze *et al.*, 2004). Seedlings were treated with purified EVs isolated from *Pto* DC3000 cultures, and GUS staining was measured after 18 h. We observed a significant induction of *pFRK1*::GUS expression triggered by the EVs albeit lower when compared to flg22 treatments (Fig. 4B, 4C). EV-induced *FRK1* upregulation is in agreement with previous observations (Bahar *et al.*, 2016). We also tested whether treatment with *Pto* DC3000 EVs could arrest seedling growth, a prototypic PTI response of plants to continual MAMP stimulation (Bredow *et al.*, 2019). Unexpectedly, we observed no significant growth

246 reduction (Fig. 4D). This suggests that immune induction by *Pto* DC3000 EVs does not affect
247 plant growth, unlike treatment with flg22 (Fig. S4B) (Bredow *et al.*, 2019).
248
249 A previous study demonstrated that bacterial (*X. campestris*) EV activation of *FRK1* expression
250 depends on the EF-Tu Receptor (EFR), which is responsible for detection of the immunogenic
251 peptide elf18 derived from bacterial EF-Tu (Bahar *et al.*, 2016, Zipfel *et al.*, 2006). To
252 determine the pathway, by which the *Pto* DC3000 EVs trigger immune responses, we treated
253 *efr-1* and *flagellin sensing 2* (*fls2*) mutants, the latter responsible for recognition of the
254 immunogenic peptide flg22 of bacterial flagellin in *A. thaliana* (Zipfel *et al.*, 2004), with *Pto*
255 DC3000 EVs and monitored *FRK1* gene expression. The *Pto* DC3000 EVs triggered *FRK1*
256 gene expression in wild type and *efr-1* mutants to similar levels (Fig. 4E). No *FRK1* induction
257 was observed in *fls2* mutants. Thus, the EVs isolated from *Pto* DC3000 cultures must contain
258 bacterial flagellin. Notably, SEM analysis of gradient enriched EV samples showed the co-
259 purification of filament-like structures (Fig. 1B), which could represent detached bacterial
260 flagellar or pili. This suggests that co-purifying flagellin molecules may trigger plant immune
261 responses.
262

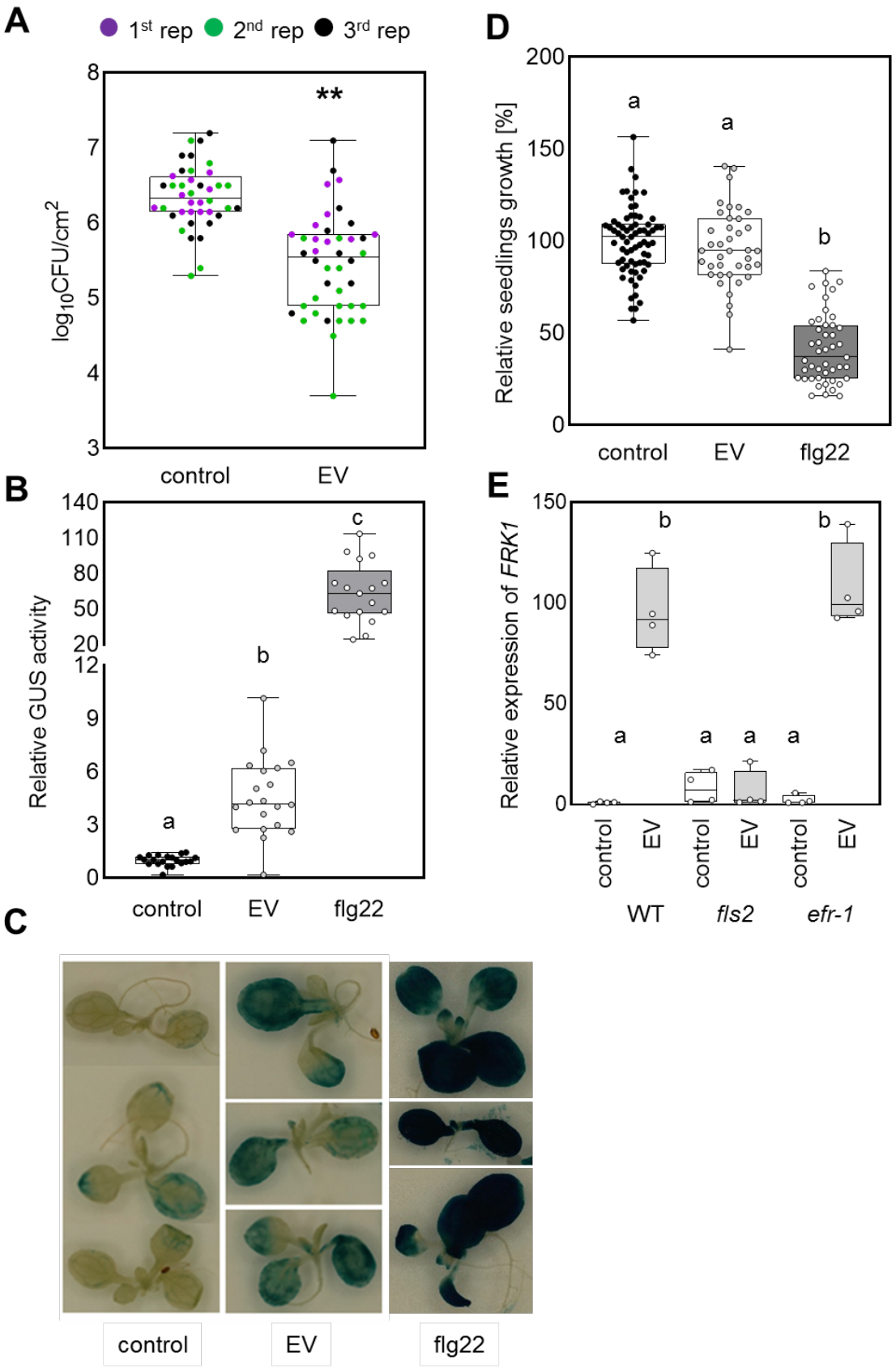

Figure 4. Immunogenic effects of *Pto* DC3000 EVs. A) *Pto* DC3000 growth (CFU) after infection into leaves of *A. thaliana* without and with EV pre-treatment at 3 dpi (control = 0.02 mM EDTA). Three biological repeats consisting each 12 independent samples were

performed. The dots with the same colour represent independent samples from one biological repeat. **B)** Quantification of *pFRK1*::GUS activity in seedlings incubated without and with EVs (concentration ≈ 1.10^{10}) or with 100 nM flg22 for 18 h. **C)** Representative pictures of *pFRK1*::GUS seedlings incubated without and with EVs (concentration ≈ 1.10^{10}) or with 100 nM flg22 for 18 h. **D)** Fresh weight of seedlings grown without and with EVs (concentration ≈ 1.10^{10}) for 8 days. For control n = 69; for 100 nM flg22 treatment n = 44 and for EV treatment n = 39 of independent samples. **E)** Relative *FRK1* gene expression in seedlings of the indicated genotypes incubated without and with EVs (concentration ≈ 1.10^{10}) for 5 h (control = 0.02 mM EDTA), four independent samples were used for each variant. For A, B, D, E each dot in the boxplot represents an independent sample. The box in boxplots extends from 25th to 75th percentiles, whiskers go down to the minimal value and up to the maximal value, the line in the middle of the box is plotted at the median. Asterisks indicate statistical significances (two tailed Welsch´s t-test; $p < 0.01$) in A; different letters indicate significant differences (Welsch´s ANOVA with Dunnett´s T3 multiple comparisons post hoc test; $p < 0.05$)) in B, D and E.

EVs from cultured *Pto* DC3000 are enriched in proteins with predicted roles in transport and antimicrobial peptide resistance

To gain insights into the function of *Pto* DC3000 EVs during the infection process, we characterized the proteome of EVs using liquid chromatography-based tandem mass spectrometry (LC-MS/MS). The *Pto* DC3000 EV-associated proteins were isolated from planktonic *Pto* DC3000 cultures by gradient enrichment. The proteomes of whole cells (WC) (Park *et al.*, 2014) and the outer membrane (OM) (Choi *et al.*, 2011) from bacteria grown to late exponential phase (OD_{600} = 3-4; Fig. S2B) were also analysed and compared with the EV proteome. As expected, we detected the most proteins from the WC sample (n = 1587), followed by the EV sample (n = 890) and 212 proteins in OM samples (Fig. 5A, Table S1). In total, 2898 proteins were identified over all samples, of which 1899 proteins were identified at least in three samples per sample type (WC, EV or OM). These proteins were taken forward for further analysis (Table S1). Similar protein intensity distributions were obtained for all samples (LFQ values were generated by MaxQuant, Fig. S5) and the four replicate measurements per sample type fell into sample clusters on the first and second principal components, suggesting a systematic difference in the proteomes of these three sample types (Fig. 5B). By comparing the proteomes of EV and WC, we identified 369 EV-enriched proteins, consisting of 162 proteins

281 exclusively identified in at least three replicates of EV sample (EV unique; Fig. 5C) and 207
282 proteins significantly higher in the EV compared with WC (Fig. 5C; Table S1).
283
284 Of the nine labelled highly-enriched EV and the five EV-unique proteins (Fig. 5C), eight have
285 unknown subcellular localization (PSPTO_3807; PSPTO_4822; PSPTO_0894; PSPTO_3407;
286 PSPTO_3424; PSPTO_3970, PSPTO_3396; and PSPTO_3409). This could indicate that these
287 proteins are predominantly present in EVs, a localization not included in the predictions. Four
288 proteins are annotated as lipoproteins, reported in other Gram-negative bacteria to mediate the
289 cross-linking of the peptidoglycan (PG) layer with the OM and thus playing roles in the
290 production of OMVs (Schwechheimer and Kuehn, 2015). PSPTO_3409 is the locus tag for the
291 ATP-dependent ClpP-1 protease. Clp proteases were previously shown to regulate quorum
292 sensing, in turn affecting OMV production and biofilm formation (Figaj *et al.*, 2019, Hall *et al.*,
293 2017). The other were annotated as hypothetical proteins.
294
295 The EV-enriched proteome included proteins related to virulence (Fig. 5C, Table S1), such as
296 MucD (PSPTO_4221) (Wang *et al.*, 2019), HopAJ2 (PSPTO_4817) (Vinatzer *et al.*, 2006) and
297 HopAH2-2 (PSPTO_3293) (Lovelace *et al.*, 2018, Schechter *et al.*, 2006). A major function of
298 virulence proteins is the suppression of PTI (Block & Alfano, 2011). To test whether *Pto*
299 DC3000 EVs could suppress a prototypic PTI response, we pre-treated leaves with EVs from
300 cultured bacteria 24 h before eliciting a ROS burst with MAMPs (flg22, elf18). EV pre-
301 treatments neither significantly reduced nor increased the MAMP-induced ROS production
302 (Fig. 6A). This suggests that under the tested conditions, *Pto* DC3000 EVs are not
303 predominantly involved in immune inhibition and/or further enhancing MAMP responses.
304

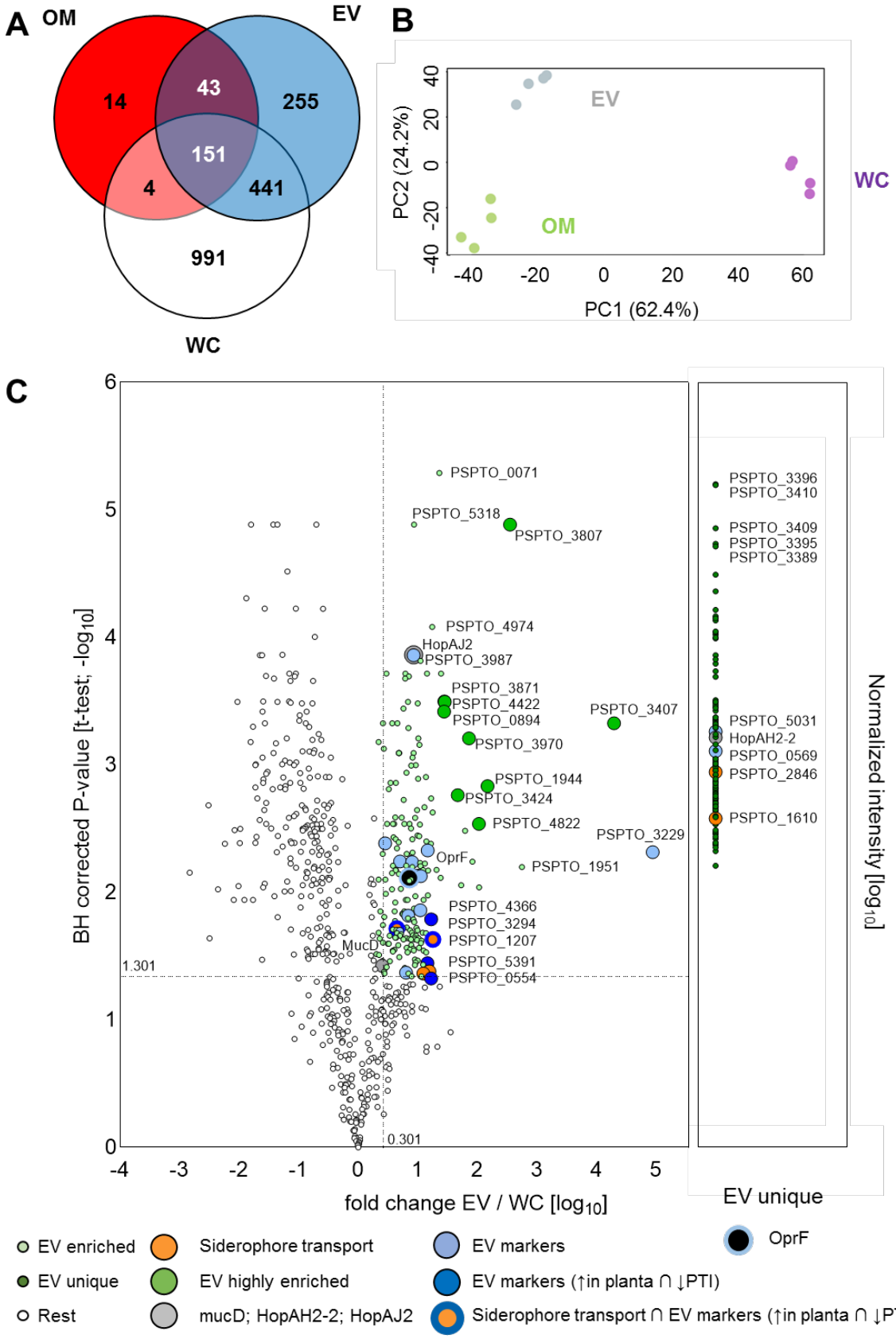

Figure 5. Proteomic analysis identifies 369 proteins enriched in *Pto* DC3000 EVs. A) Comparison of proteins detected in *Pto* DC3000 whole cell lysate (WC), outer membrane (OM) and extracellular vesicles (EV). **B)** Principal Component Analysis (PCA) analysis of

identified proteins **C)** Volcano plot comparing EV and WC proteomes. EV-enriched proteins were defined in two categories: I) fold change EV/WC > 2 & FDR < 0.05 (t-test); II) measured in three replicates in EV but not in WC. In addition, the mean intensity in EV protein needs to be in the top 50% of all proteins, so only high intensity proteins in EV are selected. Four types of proteins enriched or unique in EVs were highlighted: proteins related to virulence; proteins related to siderophore transport; candidate EV biomarkers, and proteins highly enriched in EVs compared with WC.

Next, we performed a gene set analysis on the 369 EV-enriched proteins to examine the biological processes (from gene ontology (GO) (Ashburner *et al.*, 2000, The Gene Ontology, 2019) and pathways (KEGG (Kanehisa *et al.*, 2010)), in which these proteins are involved. In total ten GO biological processes were signficantly enriched (FDR < 0,05; DAVID bioinformatics resources (Huang da *et al.*, 2009a, Huang da *et al.*, 2009b)), out of which six were connected with the general process "transport", including transmembrane transport, intracellular transmembrane transport, protein secretion, siderophore transport and protein transport by the Sec complex (Fig. 6B; Table S2). Nine KEGG categories, including cationic antimicrobial peptide resistance, β-lactam resistance and bacterial secretion system are significantly enriched in EVs (Fig. 6B, Table S2).

We used available *Pto* DC3000 proteome and transcriptome data to examine the *in planta* responses of the EV-enriched proteins (Nobori *et al.*, 2018, Nobori *et al.*, 2020). Comparison with the proteome data showed that of the 369 EV-enriched proteins 78 (21 %) are modulated *in planta* and 48 (13 %) are modulated in immune deficiency mutants (Fig. 6C, Table S3). Of the 369 genes coding for EV-enriched proteins, 98 genes (27 %) were differentially transcribed *in planta* compared to cultured bacteria and 166 genes (45 %) responded to the induction of PTI (Fig. 6D, Table S3). Most EV-unique and EV-highly enriched proteins were transcriptionally upregulated *in planta* whereas the majority of the genes of all identified proteins (WC, OM and EV) were downregulated *in planta* (Fig. 6E). When focussing on GO terms, we found that genes connected with the general process "transport" responded strongly to *in planta* conditions upon

327 PTI activation (Fig. 6B). Interestingly, all genes connected with siderophore transport were
328 strongly upregulated in response to *in planta* conditions, but downregulated *in planta* upon
329 activation of PTI (Fig. 6B, Table 1). Thus, during sucessful infection the significant enrichment
330 of siderophore transport proteins at EVs may suggest a role for EVs in iron or other metal ion
331 acquisition (Fig. 5C, orange labelling). When focussing on KEGG pathways, genes connected
332 with protein export (seven out of nine), secretion systems (eight out of eleven), chemotaxis (ten
333 out of twelve) and flagellar assembly (eight out of eight) were affected *in planta* in response to
334 PTI (Fig. 6B).
335

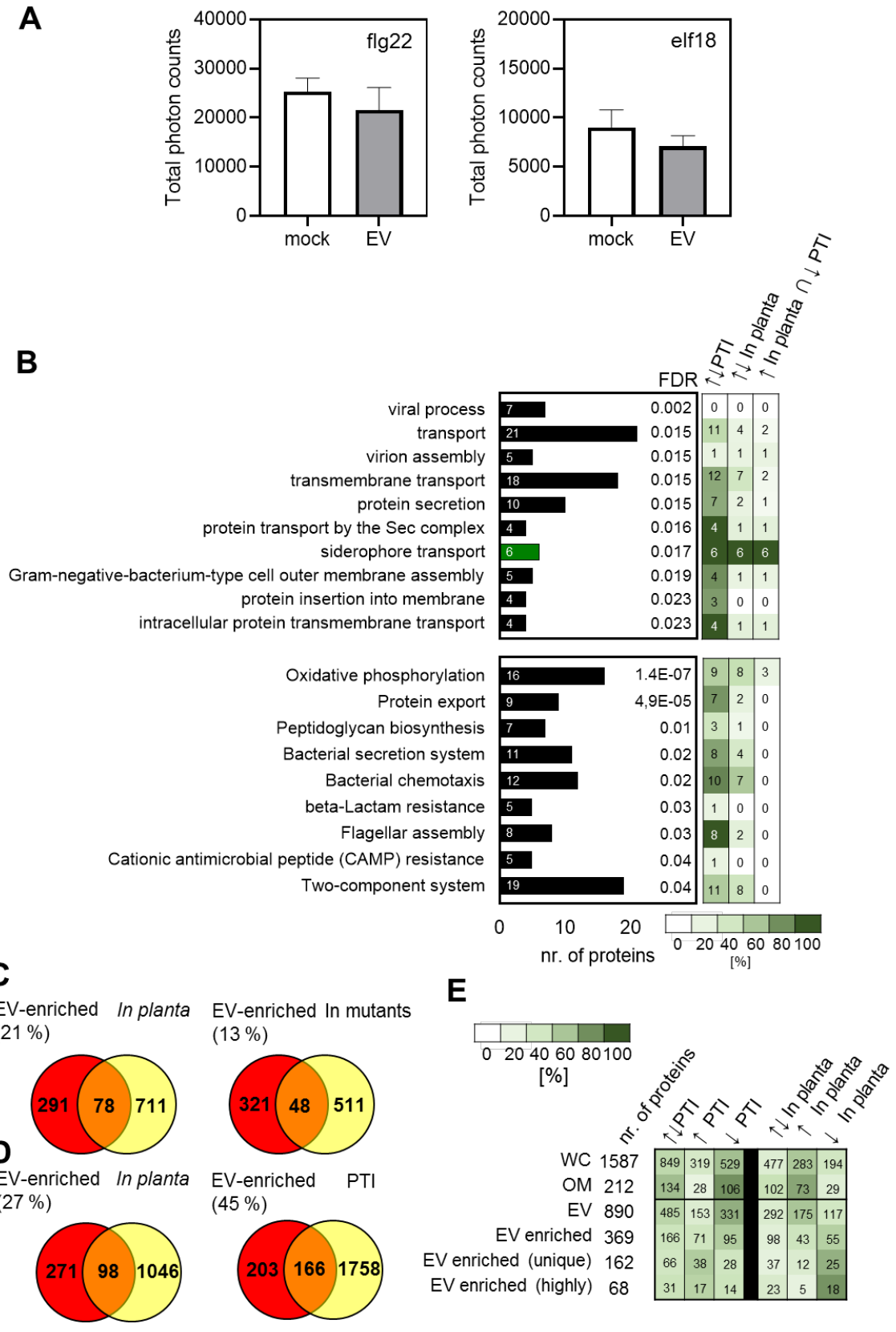

Figure 6. Protein profiles of EVs suggest functions other than classical immune suppression. A) Quantification of MAMP-induced ROS in leaves treated without and with EVs (concentration ≈ 1.10^{10}) for 24 h. The bars represent mean and error bars represents SEM from n = 12. **B)** Enriched proteins in GO biological processes and KEGG categories in EV-

enriched proteins. The heat-map represents the transcriptional profile based on the comparison of our data with transcriptomic data from (Nobori *et al.*, 2018) of genes encoding proteins identified by GO enrichment analysis. The intensity of green colour represents the percentage of affected genes and numbers in boxes represent the exact number of affected proteins. The arrows indicate transcriptional up- and downregulation. **C)** The Venn diagram represents the number of genes encoding EV-enriched proteins that are transcriptionally regulated *in planta* and responding to immune-deficient *in planta* conditions (Nobori et al. 2020). **D)** Transcriptional regulation of *Pto* DC3000 genes encoding EV-enriched proteins *in planta* and responding to PTI (Nobori *et al.*, 2018). **E)** The heat-map represents the transcriptional regulation of genes encoding identified proteins by proteome analysis *in planta* and responding to PTI (Nobori *et al.*, 2018).

Table 1 *In planta* transcription[1] of genes coding proteins enriched in EVs belonging to GO:siderophore transport

Locus tag	Subcellular Localization	Product Description	Gene transcription		other
			*In planta**	PTI**	
PSPTO_1207	Outer Membrane	iron(III) dicitrate transport protein fecA	↑	↓	EV marker
PSPTO_1610	Outer Membrane	TonB-dependent siderophore receptor	↑	↓	EV unique
PSPTO_2152	Outer Membrane	TonB-dependent siderophore receptor	↑	↓	
PSPTO_2846	Outer Membrane	TonB-dependent siderophore receptor	↑	↓	EV unique
PSPTO_3294	Outer Membrane	TonB-dependent siderophore receptor	↑	↓	EV marker
PSPTO_3574	Outer Membrane	TonB-dependent siderophore receptor	↑	↓	

[1] Nobori et al. 2018. Increased (↑) or decreased (↓) gene transcription *in planta* vs *in vitro** or under induced PTI *in planta* vs non-induced PTI *in planta***.

Pto DC3000 appears to release EVs in the form of OMVs and OIMVs

Classification of the proteins enriched in EVs by putative subcellular localization revealed distinct localization profiles compared with WC and OM proteins. While 66 % of WC proteins were cytoplasmic, about half (51 %) of the EV-enriched proteins were cytoplasmic membrane-associated, with the next largest known class being OM-associated (11 %) (Fig. 7A). Yet, being putative localizations, we cannot exclude the possibility of other/additional localizations of the proteins as currently predicted, in particular for anchor-less proteins. Because the localization profile of the EV-enriched protein suggested that *Pto* DC3000 produces EVs in the form of OIMVs (Perez-Cruz *et al.*, 2015), we performed additional transmission electron microscopy (TEM) analysis of *Pto* DC3000 bacteria. Micrographs of the sectioned samples showed several structures reminiscent of budding vesicles from the bacterial outer membrane (Fig. 7B, 7C). Combining the data from proteomics and TEM, it may suggest that *Pto* DC3000 produces EVs

350 in the form of both OMVs and OIMVs, as previously described for the closely related species

351 *Pseudomonas aeruginosa* (Toyofuku *et al.*, 2019).

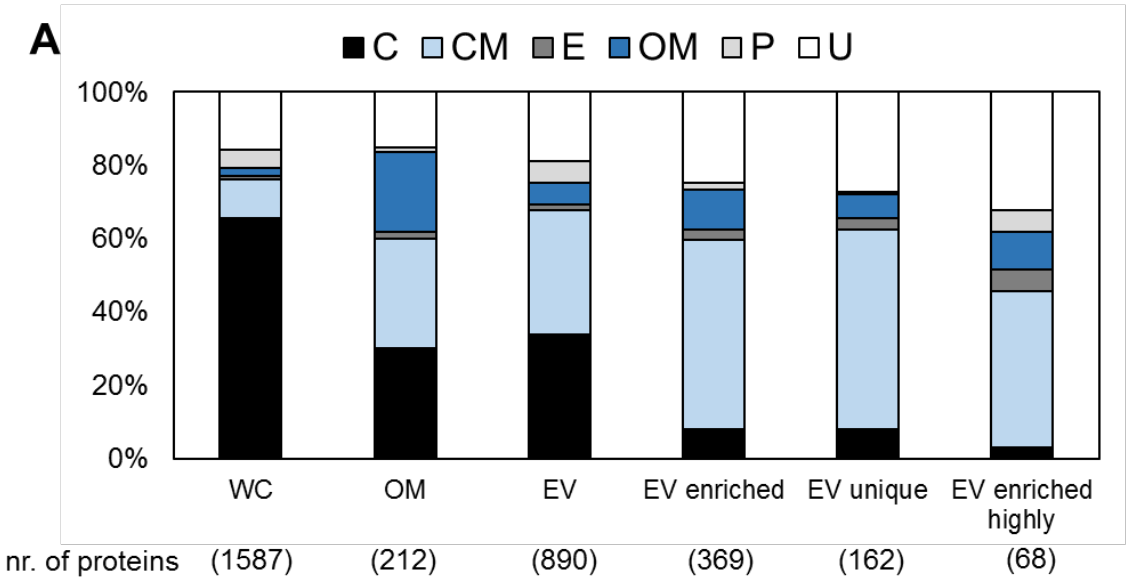

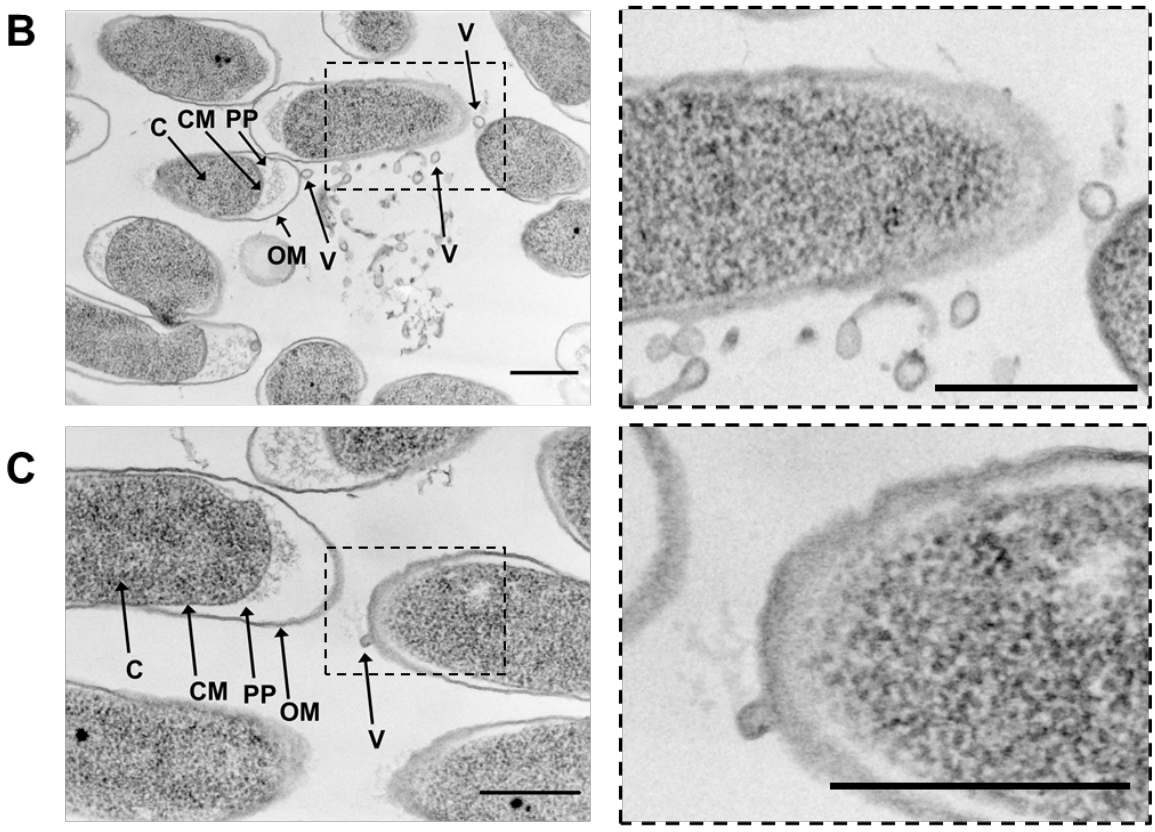

Figure 7. Localization profiles of EV proteins and TEM analysis suggest the release of *Pto* DC3000 EVs in the form of OMVs and OIMVs. A) Predicted protein localization of identified in whole cell lysate (WC), outer membrane (OM), EVs, EV-enriched, EV unique (the proteins identified only in EVs not in WC) and EV enriched – highly (protein which FDR < 0.005 and EV/WC > 20) in [%]. **B-C)** The left panel shows representative TEM micrographs from planktonic *Pto* DC3000 cultures (OD_{600} = 3-4). C, cytoplasm; CM,

cytoplasmic membrane; OM, outer membrane; PP, periplasm; V, vesicle. All scale bars = 500 nm. **B)** A lot of smaller and larger vesicles in proximity to cells. It is important to note that the larger vesicle-like structures could also represent debris of death cells. **C)** Budding vesicle in the right part of the micrograph. Dashed boxes indicate enlarged regions of the micrographs shown in the right panel.

352

353 **Comparative analysis of proteomic data revealed 20 candidates for *Pto* DC3000 EVs**
354 **markers**

355 Since a number of EV proteomes have been reported from *P. aeruginosa* (Couto N. *et al.*, 2015,
356 Choi *et al.*, 2011, Reales-Calderon *et al.*, 2015), we addressed whether the protein composition
357 of EVs from *Pto* DC3000 and *P. aeruginosa* PAO1 (*Pa* PAO1) share similarities. We focussed
358 on three published *Pa* PAO1 EV proteomes and found that 103 proteins were identified in the
359 EV proteomes across the three reports (Couto N. *et al.*, 2015, Choi *et al.*, 2011, Reales-Calderon
360 *et al.*, 2015). Of the 103 shared EV proteins from *Pa* PAO1, we could identify 100 orthologous
361 proteins encoded in the *Pto* DC3000 genome and 44 proteins were enriched in *Pto* DC3000
362 EVs (Table S4). We refer to these as the EV "core". These proteins were highly enriched in
363 localization to the outer membrane (44 %) and cytoplasmic membrane (26 %) (Fig. 8A),
364 consistent with EVs released in the form of OMVs (Fig. 7B, 7C). From these 44 proteins, 20
365 were putative outer membrane-localized proteins and thus represent good candidate biomarkers
366 for the detection of EVs (Table 2, S4; Fig. 5C blue labelling). Interestingly, 20 out of 31 proteins
367 with predicted membrane localization (20 out of 31) were transcriptionally regulated *in planta*
368 in response to PTI activation (Nobori *et al.*, 2018), of which 14 showed downregulation.
369 Overall, twelve of the 31 proteins responded transcriptionally to the *in planta* condition, with
370 nine showing upregulation (Fig. 8B).

371

372 One of the predicted EV markers is OprF (Outer membrane porin OprF; Fig. 5C black
373 labelling), which we used for immunodection of *Pto* DC3000 EVs *in planta* and purified from
374 *Pto* DC3000 cultures. Using *anti*-OprF antibodies, we identified specific bands in filtered

375 apoplastic fluids of *A. thaliana* leaves infected with *Pto* DC3000 at two and three days post
376 infection but not in control treated plants (Fig. 8C). This provides additional evidence that *Pto*
377 DC3000 releases EVs *in planta* during infection.
378

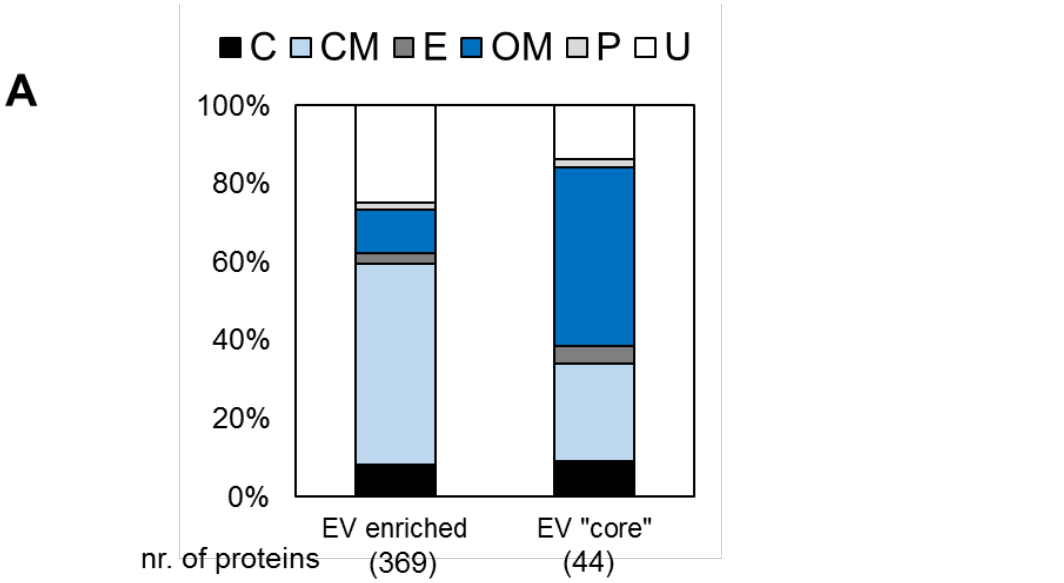

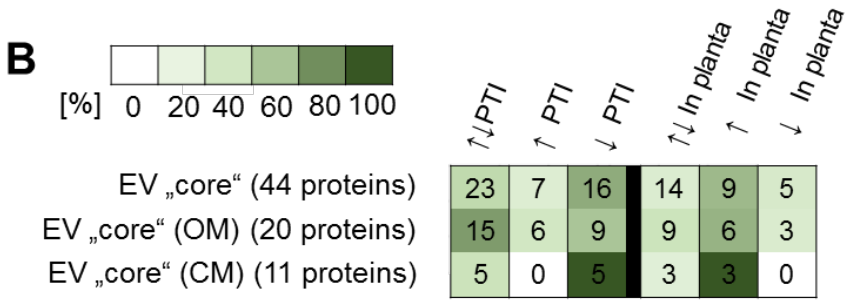

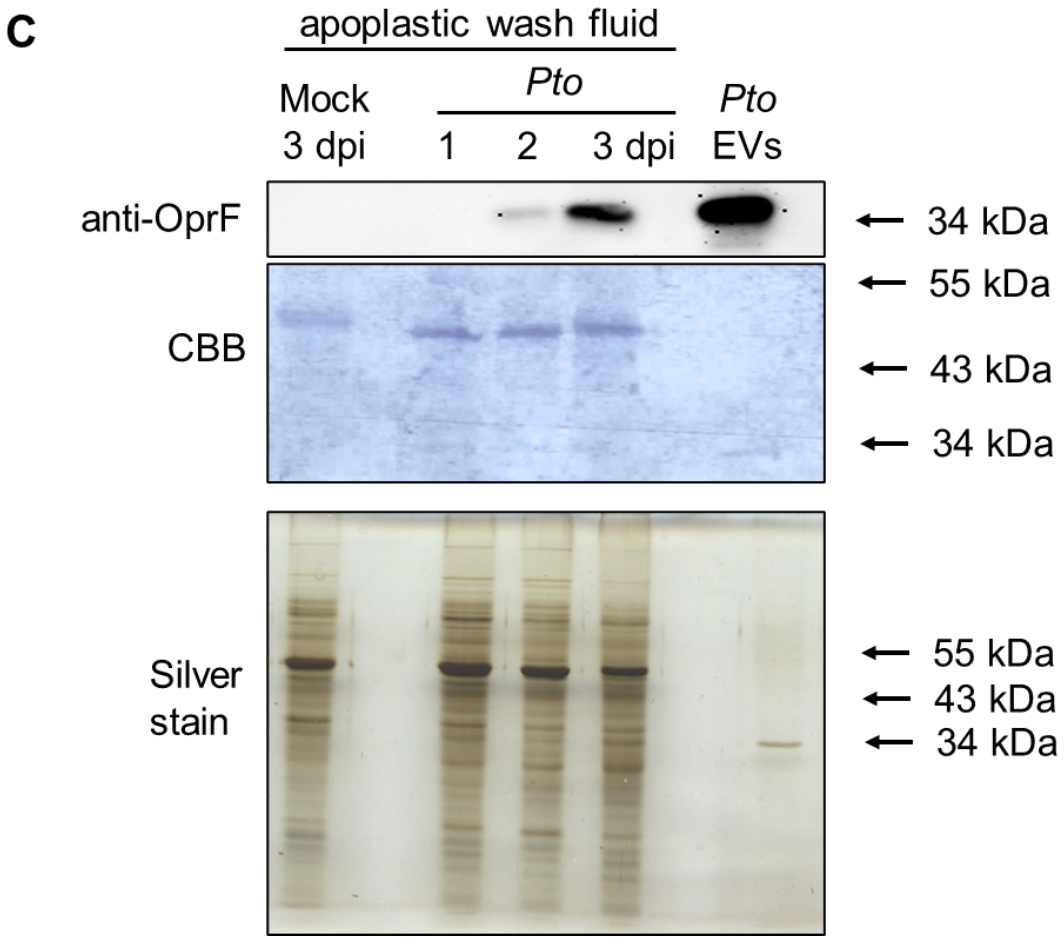

Figure 8. Prediction of Pseudomonas "core" EVs proteins identifies biomarkers for the detection of *Pto* DC3000 EVs *in planta*. A) Predicted protein localization of the *Pto* DC3000 EV enriched proteins whose orthologs are found in *P. aeruginosa* EV proteomes [%] total number of identified proteins is 44. **B)** Heat-map representing transcriptional changes in genes encoding *Pseudomonas* "core" EV proteins, EV "core" proteins localized on outer membrane (OM) and EV "core" proteins localized on cytoplasmic membrane (CM). The intensity of green colour represents percentage of affected genes and the numbers in boxes show the exact number of affected genes. **C)** Immunoblot monitoring OprF, a predicted *Pto* DC3000 EV biomarker, in EVs collected from apoplastic fluids. OprF antibodies detect bands in apoplastic fluids from *A. thaliana* infected with *Pto* DC3000 and in gradient enriched EVs. Coomassie Brilliant Blue (CBB) and silver staining are shown as loading control.

379

380

Table 2 *In planta* transcription[1] of genes coding proteins suggested as promising candidates to be EV markers

				Gene expression			
Locus Tag	**UniProt ID**	**Subcellular Localization**	**Name**	**PTI***	**In planta****	**other**	
PSPTO_0554	Q88A43	Outer Membrane	organic solvent tolerance protein	↓	↑		
PSPTO_0569	Q88A28	Outer Membrane	autotransporting lipase, GDSL family	↑	n.s.	EV unique	
PSPTO_1207	Q887S9	Outer Membrane	iron(III) dicitrate transport protein fecA	↓	↑	Siderophore transport	
PSPTO_1296	Q887J6	Outer Membrane	porin B	↑	n.s.		
PSPTO_1437	Q886Y7	Outer Membrane	lysyl-tRNA synthetase	↓	n.s.		
PSPTO_1542	Q886N5	Outer Membrane	outer membrane protein	↓	n.s.		
PSPTO_1720	Q885W1	Outer Membrane	outer membrane protein	↑	↓		
PSPTO_2272	Q883S8	Outer Membrane	outer membrane lipoprotein Oprl	n.s.	↓		
PSPTO_2299	Q883Q1	Outer Membrane	outer membrane porin OprF	n.s.	↑		
PSPTO_3229	Q880E1	Outer Membrane	filamentous hemagglutinin, intein-containing	↑	↓		
PSPTO_3294	Q87ZX8	Outer Membrane	TonB-dependent siderophore receptor	↓	↑	Siderophore transport	
PSPTO_3971	Q87Y41	Outer Membrane	peptidoglycan-associated lipoprotein	n.s.	n.s.		
PSPTO_3987	Q87Y25	Outer Membrane	porin D	n.s.	n.s.	beta-Lactam resistance	
PSPTO_4115	Q87XR1	Outer Membrane	lipoprotein SlyB	↑	n.s.		
PSPTO_4366	Q87X24	Outer Membrane	iron-regulated protein A	↓	↑		
PSPTO_4839	Q87VU6	Outer Membrane	hypothetical protein	↑	n.s.		
PSPTO_4940	Q87VJ6	Outer Membrane	hflK protein	↓	n.s.		
PSPTO_4977	Q87VG0	Outer Membrane	outer membrane efflux protein ToIC	↓	n.s.	Bacterial secretion system; Lactam resistance; antimicrobial peptide (CAMP) resistance	beta-Cationic
PSPTO_5031	Q87VA8	Outer Membrane	type IV pilus biogenesis protein PilJ	n.s.	n.s.	EV unique	
PSPTO_5391	Q87UB4	Outer Membrane	outer membrane porin, OprD family	↓	↑		

[1] Nobori et al. 2018. Increased (↑) or decreased (↓) gene transcription *in planta* vs *in vitro** or under induced PTI *in planta* vs non-induced PTI *in planta***. n.s. = non-significant

Discussion

Bacterial EVs have been widely studied for their content and biological importance in various human diseases. Until recently, however, EV production by phytopathogenic bacteria has been mostly disregarded (Rybak & Robatzek, 2019). In the past few years, the attention in plant-microbe interactions has turned slowly towards EV signalling. EV production by phytopathogenic bacteria was shown for *A. tumefaciens* C58, *Xanthomonas campestris* pv *campestris* (*Xcc*), *X. campestris* pv *vesicatoria*, *Pto* T1, *Pto* DC3000 and *Xyllela fastidiosa* subsp. *fastidiosa* Temecula-1, subsp. *pauca* 9a5c and subsp. Fb7 (Bahar *et al.*, 2016, Feitosa-Junior *et al.*, 2019, Chowdhury & Jagannadham, 2013, Ionescu *et al.*, 2014, Knoke *et al.*, 2020, McMillan *et al.*, 2020, Sidhu *et al.*, 2008, Sole *et al.*, 2015). In this study, we provide several pieces of evidence for the role of EVs in the interaction of *Pto* DC3000 with plants: i) the bacteria produce EVs *in planta* during infection; ii) proteins responding to the plant environment are enriched in EVs; iii) known MAMPs and effectors are associated with EVs; and iv) plants respond to EVs with prototypic PTI reactions.

We show that *Pto* DC3000 produces spheres bulging from its outer membrane and releases spherical vesicles into the environment (Fig. 1A, 7B, 7C). Our data indicate the production of EVs predominantly in the form of OMVs albeit the predicted localization profiles of the EV-enriched proteins also suggest OIMV production (Fig. 7A, 7B, 7C, 8A), both representing well-established routes of vesicle release in Gram-negative bacteria (Toyofuku *et al.*, 2019). The more polydisperse size seen for EVs recovered from apoplastic fluids of susceptible *Pto* DC3000 infected plants could not only represent a mixed pool of plant and bacterial derived EVs, but also suggests that *Pto* DC3000 might release EVs from different biogenesis routes including membrane blebbing and explosive cell lysis.

406 Our results suggest the regulated production of EVs and the specific enrichment of proteins to
407 EVs. *Pto* DC3000 cultures produced more EVs with increasing bacterial density during
408 exponential-phase growth, showing a correlation between bacteria and EV numbers (Fig. 1E).
409 The production of EVs by *Pto* DC3000 was slightly responsive to bacterial growth style and
410 isolation technique. EVs produced from biofilm *Pto* DC3000 and fluid planktonic culture were
411 smaller and more negatively charged than gradient enriched planktonic EVs. Moreover, heat
412 inactivation of bacteria increased vesicle numbers and size (Fig. 1D, 1F). Since EVs from heat
413 inactivated bacteria did not differ in charge profiles compared to untreated EVs (Fig. S6D), it
414 is possible that explosive cell lysis contributes to the higher EV numbers (Toyofuku *et al.*,
415 2019). Turnbull *et al*. demonstrated that explosive cell lysis of a sub-population of cells from *P.*
416 *aeruginosa* biofilms results in the generation of bacterial EVs (Turnbull *et al.*, 2016).
417 Furthermore, heat shock stimulates the release of OMVs, most likely a result of high levels of
418 un- and misfolded proteins accumulating in heat-stressed cells (Macdonald & Kuehn, 2013,
419 McBroom & Kuehn, 2007). In this context it is interesting to note that the biophysical
420 characteristics of *Pto* DC3000 EVs remained largely unchanged under disruptive treatment
421 conditions except boiling (Fig. 2). Thus, the EVs from *Pto* DC3000 are stable and can maintain
422 functionality as reported previously for other bacteria (Alves *et al.*, 2016, Arigita *et al.*, 2004,
423 Frank *et al.*, 2018).
424
425 A range of activities has been associated with bacterial EVs. This includes modulation of host
426 immunity i.e. through EVs presenting MAMPs and delivering effector molecules (Bahar *et al.*,
427 2016, Schwechheimer & Kuehn, 2015). We found that EVs from *Pto* DC3000 cultures elicited
428 a robust induction of the *FRK1* defence marker gene (Fig. 4B, 4C, 4E). Compared with EVs
429 from *Acidovorax* and *Xanthomonas* bacteria, *Pto* DC3000 EVs provoked a modest induction of
430 defence gene expression (Bahar *et al.*, 2016). Despite this, the *Pto* DC3000 EVs did not trigger

a growth arrest in Arabidopsis seedlings (Fig. 4D). These results suggest that the immunogenic activities of the EVs, but not a longer-term trade-off with growth, may be relevant in their interaction with plants. In contrast to our results, McMillan et al. reported significant seedling growth repression in response to *Pto* DC3000 EVs (McMillan *et al.*, 2020). This disparity in results may be due to several factors, including differences in the growth conditions of both the bacterial cultures and the *A. thaliana* seedlings, the type of biochemical isolation of EVs and vesicle dose. That EVs can serve as protective vaccines has been reported for many bacteria but not phytopathogens. We show here that plants pre-treated with *Pto* DC3000 EVs were modest, yet significantly protected against subsequent infection with *Pto* DC3000 bacteria (Fig. 4A). Consistently, EV pre-treatments did not inhibit a MAMP-induced ROS burst (Fig. 6A). The stronger protective immune response observed by McMillan et al. may be due to differences in experimental procedures, as noted above (McMillan *et al.*, 2020). In addition, McMillan et al. showed that pre-treatment with bacterial EVs provided protection against subsequent oomycete infection (McMillan *et al.*, 2020). The potential for *Pto* DC3000 EVs to induce broad-spectrum resistance supports a role for PTI.

PTI responses to *Pto* DC3000 involve recognition by FLS2, EFR and LIPO-OLIGOSACCHARIDE-SPECIFIC REDUCED ELICITATION (LORE), which detect immunogenic flg22, elf18 and 3-OH-FAs (Wan *et al.*, 2019). EVs from bacterial phytopathogens are enriched in EF-Tu and LPS (Bahar *et al.*, 2016, Feitosa-Junior *et al.*, 2019, Sidhu *et al.*, 2008), suggesting the presence of elf18 and 3-OH-FAs. Bahar *et al*. demonstrated that BRI1-ASSOCIATED KINASE 1 (BAK1) and SUPPRESSOR OF BIR 1 (SOBIR1), interacting co-receptors of PRRs, mediate the immunogenic perception of EVs from *X. campestris* pv. *campestris* (Bahar et al., 2016). We show that our vesicle samples from *Pto* DC3000 elicit immune responses that are dependent on FLS2 (Fig. 4E). Despite depleting

456 extracellular components from EV samples by density gradient centrifugation, it is possible that
457 flagella co-purify with the *Pto* DC3000 EV samples, since filamentous structures were observed
458 in SEM analysis (Fig. 1B). Contamination of flagella in EVs was reported to contribute to the
459 detection of FliC in EVs from *P. aeruginosa* (Bauman & Kuehn, 2006). However, flagella
460 proteins such as FliC have a specific affinity for EVs and are involved in EV production in
461 *Escherichia coli* (Manabe et al., 2013). We cannot exclude that flagella proteins play roles in
462 EV production in *Pto* DC3000, evidenced by the finding that six flagella-associated proteins
463 were enriched in *Pto* DC3000 EVs (Table S1).
464
465 Why *Pto* DC3000 produces EVs during infection is unclear. It is evident that the plant apoplast
466 represents a stressful environment for its colonizing bacteria. Bacteria respond to environmental
467 stress with the production of EVs, which allows for cell surface remodelling, secretion of
468 degraded and damaged cargo, and uptake of nutrients in bacterial communities i.e. by packaging
469 transporters in EVs (Schwechheimer & Kuehn, 2015, Toyofuku *et al.*, 2019, Zingl *et al.*, 2020).
470 As the growth state of bacteria determines the nutrient availability, the production of EVs could
471 support the growth of *Pto* DC3000 in culture and *in planta*. Proteomics analysis of gradient
472 enriched *Pto* DC3000 EVs identified 890 vesicle-associated proteins, of which 369 were
473 enriched in the EVs relative to the cellular proteome (Fig. 5, Table S1). The mechanisms by
474 which this enrichment occurs suggests a selective delivery of cargo into the EVs and should be
475 investigated in the future. Of the EV-enriched proteins, six out of ten GO biological process
476 categories were related to transport mechanisms (Fig. 6B). Proteins involved in siderophore
477 transport were enriched in the EVs and have recently been shown to play a role in *Pto* DC3000
478 infection success (Nobori *et al.*, 2018). Interestingly, the expression of genes coding for all
479 siderophore transport proteins enriched in EVs was upregulated *in planta* compared to *in vitro*
480 conditions as well as downregulated upon induction of PTI (Fig. 6B; Table 1) (Nobori *et al.*,

2018). Thus, regulation of siderophore transport proteins can be considered as an adaptive response of *Pto* DC3000 to iron/metal ion availability, and secretion into EVs may allow improved acquisition of iron, analogous to EV secretion of the siderophore mycobactin in *Mycobacterium tuberculosis* (Prados-Rosales et al., 2014). The plant's apoplast, which is the niche colonized by *Pto* DC3000 represents an environment where bacteria are challenged with iron acquisition and plant defence molecules (Nobori *et al.*, 2018). The role of bacterial EVs in metal acquisition is not restricted to iron. *Neisseria meningitidis* produces OMVs, which are enriched in zinc acquisition proteins (Lappann *et al.*, 2013), and zinc regulates siderophore biosynthesis genes in *Pseudomonas fluorescens* (Rossbach et al., 2000). It is thus feasible that *Pto* DC3000 produces EVs to help it adapt to metal conditions in the environment including the plant's apoplast.

The hypothesis that *Pto* DC3000 uses EVs to adapt to the growth environment is supported by our finding that *Pto* DC3000 EVs are enriched in proteins related to the KEGG categories β-lactam resistance and cationic antimicrobial peptide resistance (Fig. 6B). Several studies demonstrated that EVs can improve bacterial survival during antibiotic exposure. *Stenotrophomonas maltophilia* produced more EVs upon treatment with the β-lactam antibiotic imipenem (Devos *et al.*, 2015, Devos *et al.*, 2017). Its EVs contained β-lactamase and increased *S. maltophilia* survival in the presence of antibiotics (Devos *et al.*, 2017). Plants defend infection by upregulation of many defence-related gene including genes coding for antimicrobial peptides (Campos *et al.*, 2018). It is possible that *Pto* DC3000 produces EVs to counter the action of plant-derived antimicrobial peptides. Collectively, we propose that *Pto* DC3000 produces EVs to improve its growth capacity both in culture and *in planta*. These findings should stimulate further studies on the role of EVs in the interaction of bacteria with plants, for example identifying the composition of EVs *in planta* using biomarkers.

Experimental procedures

Bacterial strains and growth

Pseudomonas syringae pv. *tomato* DC3000 (*Pto* DC3000) used in this study were routinely cultured at 28 °C in King's B medium containing 50 µg/mL Rifampicin at 180 rpm and on plates with 1% agar without agitation. Planktonic growth was performed in 500 mL and growth rates were measured over time as OD_{600}. Biofilm growth was measured after 24 h on plate, transferring all bacteria per plate in 10 mL 0.85% saline.

Plant material and growth conditions

Arabidopsis thaliana ecotype Columbia (Col-0), *pFRK1*::GUS (Kunze et al. 2004), *fls2c* (Zipfel et al. 2004) and *efr-1* (Zipfel et al. 2006) mutants were used in this study. For bacterial infections and ROS assays, Col-0 plants were soil-grown at 21–22 °C and 8 h photoperiod. For GUS assays, RT-qPCR analysis and induced growth arrest, seedlings were sterile grown on Murashige and Skoog (MS) plates supplemented with 1% sucrose and 1.5% gelrite (Duchefa, Netherlands) pH 5.8 for four days (after 2-4 days stratification in the dark at 4 °C), then transferred to 96-well plates containing 150 µL ½ MS medium supplemented with 1% sucrose per well and grown for eleven to twelve days in at 22 °C and 16 h photoperiod (120 – 150 $\mu E.m^{-2}.s^{-1}$).

Extraction and purification of bacterial EVs

EVs were routinely isolated from planktonic cultures at early-logarithmic to late-stationary phases as well as biofilm cultures (Fig. S2B, S2D). 100 mL of planktonic grown bacteria and 10 mL of biofilm grown bacteria, respectively, were pelleted at 4,500 x g for 2 x 20 min, the supernatant was decanted and passed through a 0.22 µm membrane (fluid samples; Fig. S2A).

Particles were pelleted from the cell-free supernatant at 100,000 x g for 1.5 h. The pellet was resuspended in 1.7 mL 1mM EDTA and loaded on sucrose density step-gradient (1.7 mL of sucrose 25%, 35%, 45%, 50%, 55%) and centrifuged at 160,000 x g for 18 h. 2 mL samples were collected from each of the sucrose density steps and diluted with 1 mM EDTA to 30 mL. Particles were pelleted at 100,000 x g for 2 h and the pellets were each resuspended in 0.16 mL 1 mM EDTA (gradient enriched samples; Fig. S2A). EV samples were immediately frozen in liquid nitrogen. Since most EVs migrated to the 55% density fraction (Fig. S6A), we then collected EVs across fractions 3 to 5, which were less variable in ζ-potential and size compared to fractions 1 and 2 (Fig. S6B, S6C).

Extraction of leaf apoplastic fluids

Apoplastic fluids were collected from leaves of six to seven weeks old plants. The leaves were cut of the rosette and vacuum infiltrated with particle-free 1 mM EDTA. After removing excess buffer, infiltrated leaves were placed into 20 mL syringes and centrifuged in 50 mL conical tubes at 900 x g for 20 minutes at 4°C. The resulting apoplastic wash was passed through a 0.22 µm membrane (apoplastic fluid samples).

EV quantification, size and charge measurements

EVs were quantified, size and charge measured by Nanoparticle Tracking Analysis (NTA) using ZetaView® BASIC PMX-120 (Particle Metrix, Germany) at room temperature. To detect EVs, we used the manufacturer's default settings for liposomes. Particle quantification and size measurements were performed by scanning eleven cell positions each and capturing 30 frames per position with the following settings: Focus: autofocus; Camera sensitivity for all samples: 85; Shutter: 100; Scattering Intensity: detected automatically. After capture, the videos were analysed by the in-built ZetaView Software 8.05.11 [ZNTA] with the following specific

556 analysis parameters: Maximum area: 1000, Minimum area 5, Minimum brightness: 25,
557 Tracelength: 15 ms. Hardware: embedded laser: 40 mW at 488 nm; camera: CMOS. For particle
558 charge measurements, the same settings were used except Minimum brightness: 30. Statistical
559 analysis was performed using either One-way ANOVA with Tukey post hoc test or Welsch´s
560 ANOVA with Dunnett´s T3 multiple comparisons post hoc test.
561
562 All samples were diluted in particle-free 1 mM EDTA buffer, checked with NTA.
563 Unconditioned King's B medium contained up to 1.4x 10^9 particles (Fig. 1D). *Pto* DC3000
564 cultures contained increasing particles numbers with cultivation time: ≈ 2.8x 10^9 particles at
565 OD_{600} = 3-4 (50% of influence); ≈ 3.7x 10^9 particles at OD_{600} = 4.5-5.5 (37% of influence), ≈
566 7*10^9 particles at OD_{600} 7.5-9 (20% of influence), and ≈1.1x 10^{10} particles at OD_{600} 10 -11
567 (13% of influence) (Fig. 1D). We therefore focused our measurements on samples collected
568 from OD_{600} > 7.5, which shows lower than 20% influence of particles from the medium (Fig.
569 1D), as well as calculated EV concentrations to the colony forming units (CFU) of the bacterial
570 cultures.
571
572 **Scanning electron microscopy**
573 Planktonic grown bacteria at OD_{600} = 3-4 and gradient enriched EVs (0.5 to 1.5x 10^{10} particles)
574 were used for scanning electron microscopy (SEM). The cells were chemically fixed using 2.5%
575 glutaraldehyde in 50 mM cacodylate buffer (pH 7.0) containing 2 mM $MgCl_2$. Then the cells
576 were applied to a glass slide, covered with a cover slip and plunge frozen in liquid nitrogen.
577 After this, the cover slip was removed and the cells were place in fixation buffer again. After
578 washing 4 times with buffer, post-fixation was carried out with 1% OsO_4 for 15 min. Two
579 additional washing steps with buffer were followed by three times washing with double distilled
580 water. The samples were dehydrated in a graded acetone series, critical-point-dried and

mounted on an aluminium stub. To enhance conductivity, the samples were sputter-coated with platinum. Microscopy was carried out using a Zeiss Auriga Crossbeam workstation at 2 kV (Zeiss, Oberkochen, Germany). The vesicle size was manually measured across five randomly selected SEM micrographs using Fiji software (Schindelin *et al.*, 2012).

Transmission electron microscopy

Planktonic grown *Pto* DC3000 at OD_{600} = 3-4 were used for ultrathin sectioning and subsequent transmission electron microscopy (TEM). The cells were concentrated by centrifugation and the cells were high-pressure frozen using a Leica HPM100 (Leica Microsystems, Wetzlar, Germany). This was followed by freeze-substitution with 0.2% osmium tetroxide, 0.1% uranyl acetate, 9.3% water in water-free acetone in a Leica AFS 2 (Leica Microsystems, Wetzlar, Germany) as described previously (Flechsler *et al.*, 2020). After embedding in Epon 812 substitute resin (Fluka Chemie AG, Buchs Switzerland), the cells were ultrathin sectioned (50 to 100 nm thickness) and post-stained for 1 min with lead citrate. Transmission electron microscopy of ultrathin sections was carried out with a JEOL F200 cryo-S(TEM), which was operated at 200 kV and at room temperature in the TEM mode. Images were acquired using a bottom-mounted XAROSA 20 mega pixel CMOS camera (EMSIS, Münster, Germany).

***Pto* DC3000 infection assay**

Overnight plate-grown *Pto* DC3000 cells were resuspended in 10 mM $MgCl_2$ and diluted to OD_{600} = 0.0006. Using a needle-less syringe, the bacterial suspension was infiltrated into mature leaves of five to six weeks old plants, three leaves per plant. For pre-treatments, , gradient enriched EVs from planktonic *Pto* DC3000 (concentration ≈ 1.10^{10}), and 0.02 mM EDTA as a negative control and 100 nM flg22 (EZbiolabs) as a positive control were syringe-infiltrated into leaves 24 h prior *Pto* DC3000 inoculation. Discs of the infected leaves (one disc per leaf,

606 0.6 cm diameter) were excised at one, two- or three-days post infection (dpi). The three leaf
607 discs from each plant were pooled and ground in 1 mL 10 mM $MgCl_2$. Serial dilutions were
608 plated on LB medium with rifampicin (50 µg/mL) and bacterial colonies were counted one day
609 after incubation at 28 ºC. Statistical analysis was performed using two tailed Welsch´s t-test.
610
611 **Histochemical β-glucuronidase (GUS) staining**
612 The histochemical GUS assay was performed with eleven day old seedlings. Seedlings were
613 treated with gradient enriched *Pto* DC3000 EVs (concentration ≈ 1.10^{10}), 100 nM flg22
614 (EZbiolabs) or as a control with 0.02 mM EDTA for 18 h. Treated seedlings were immersed in
615 X-Gluc buffer [2 mM X-Gluc (Biosynth), 50 mM $NaPO_4$, pH 7, 0.5 % (v/v) Triton-X100, 0.5
616 mM K-ferricyanide] for 16 h at 37 °C. Chlorophyll was removed by repeated washing in 80 %
617 (v/v) ethanol. Observations were made on a WHX 6000 digital microscopy (Krckova *et al.*,
618 2018).
619
620 **Fluorimetric GUS assay**
621 For fluorimetric GUS assays, eleven to twelve days old seedlings were treated with gradient
622 enriched *Pto* DC3000 EVs (concentration ≈ 1.10^{10}) or with 100 nM flg22 (EZbiolabs) or as a
623 control with 0.02 mM EDTA for 18 h. Treated seedlings were frozen in liquid nitrogen in 2 mL
624 conical tubes containing 2 clean sterile glass beads and liquid nitrogen. The frozen samples
625 were dry homogenized using a Retch mixer mill (Retch). Homogenized samples were kept on
626 ice and cold (4 °C). For total protein extraction, GUS extraction buffer was added as described
627 (Andriankaja *et al.*, 2007) [50 mM sodium phosphate (pH 7); 10 mM 2-mercaptoethanol; 10
628 mM Na_2EDTA; 0.1% Triton X-100; 0.1% sodium lauryl-sarcosine and PPIC]. GUS activities
629 were measured fluorimetrically in reaction buffer (see below) using Methylumbelliferyl-β-D-
630 glucuronic acid dihydrate (MUG), (Biosynth) as a substrate. Reaction buffer was the same

631 solution as extraction buffer with one modification: PPIC was replaced by 1 mM MUG. The
632 fluorescence was measured using TECAN fluorimeter at excitation 360 nm and emission 465
633 nm. The enzymatic activity of the sample was calculated to protein concentration measured by
634 Bradford protein assay. The absorbance was measured using TECAN spectrometer absorbance
635 at 595 nm. Statistical analysis was performed using One-way ANOVA with Tukey post hoc
636 test.
637
638 **RNA extraction and RT-qPCR analysis**
639 Gene transcription analysis was performed with twelve days old seedlings. The seedlings were
640 treated with gradient enriched EVs (concentration 1.10^{10}) and 0.02 mM EDTA as control for 3
641 h, frozen in liquid nitrogen and ground with 2.5-mm diameter silica beads using a homogenizer
642 (Retch, Germany). Total RNA was isolated using a TRIzol® reagent (Invitrogen, USA)
643 according to the manufacturer's protocol. The extracted RNA was treated with a DNA-free kit
644 (Ambion, USA). Subsequently, 1 µg of RNA was converted into cDNA with M-MLV RNase
645 H– Point Mutant reverse transcriptase (Promega Corp., USA) and an anchored oligo dT21
646 primer (Metabion, Germany). Gene transcription was quantified by qPCR using a LightCycler
647 480 SYBR Green I Master kit and LightCycler 480 (Roche, Switzerland). The PCR conditions
648 were 95 °C for 10 min followed by 45 cycles of 95 °C for 10 s, 55 °C for 20 s, and 72 °C for
649 20 s. Melting curve analyses were then carried out. Relative transcription was normalized to the
650 housekeeping gene *AtTIP41* (Czechowski *et al.*, 2005). Primers were designed using PerlPrimer
651 v1.1.21 (Marshall, 2004). The primers used are *AtFRK1*_FP, GCCAACGGAGACATTAGAG;
652 *AtFRK1*_RP, CCATAACGACCTGACTCATC. Statistical analysis was performed using One-
653 way ANOVA with Tukey post hoc test.
654
655 **Seedling growth analysis**

Four days old seedlings were transferred from MS solid media into the liquid MS media in transparent 96-well microplates. Each well contained 100 µL of media either containing 0.02 mM EDTA as a control or gradient enriched *Pto* DC3000 EVs (concentration ≈ 1.10^{10}) or with 100 nM flg22 (EZbiolabs) as a positive control. After eight days, the treated seedlings were dried using paper towel and then the fresh weight was measured. Based on the weight of each seedling relative seedlings growth [%] to control seedlings was calculated. Statistical analysis was performed using Welsch´s ANOVA with Dunnett´s T3 multiple comparisons post hoc test two tailed Student t-test.

ROS measurements

ROS production was determined using the luminol-based assay as previously described (Mersmann *et al.*, 2010). Briefly, leaves of five to six weeks old *A. thaliana* plants were infiltrated with gradient enriched EVs (concentration ≈ 1.10^{10}). After 2 h, discs were excised from the infiltrated leaves and 24 h incubated in ddH_2O at 22 °C. Then, the leaf discs were treated with 100 nM flg22 or 100 nM elf18 (EZbiolabs) to induce the production of ROS. The total photon count was collected for 45 min using a TECAN luminometer. Statistical analysis was performed using two tailed Student t-test.

Proteomics

We isolated proteins from *Pto* DC3000 whole cell lysates (WC) (Park *et al.*, 2014) and outer membrane (OM) (Choi *et al.*, 2011) as previously described. Briefly, WC and OM isolated from *Pto* DC3000 liquid culture (OD_{600} = 3-4). The cells were pelleted via centrifugation (12,000 x g for 10 min). For WC the pellet was resuspended in 1 mL of 20 mM Tris-HCl (pH 8.0), frozen in liquid nitrogen, three times thawing-freezing, and three times sonicated for 10 min at 4 °C. The samples were centrifuged at 6,000 x g for 10 min at 4 °C and supernatants were collected

and frozen in liquid nitrogen. For OM preparations, the pellet was resuspended in 1 mL 20 mM Tris-HCl (pH 8.0), sucrose (20%), followed by adding 5 uL Lysozyme (15 mg/mL) and 10 µl 0.5 M EDTA, incubation for 40 min on ice and adding 20 µL 0.5 M $MgCl_2$. After centrifugation at 9,500 x g for 20 min at 4°C, the pellet was resuspended in 1 mL ice-cold 10 mM Tris-HCl (pH 8.0) followed by sonication three times for 10 min on ice. The samples were then centrifuged at 8,000 x g for 5 min at 4 °C, washed with cold 10 mM Tris-HCl (pH 8.0), resuspend in cold, sterile MilliQ water followed by three times freezing-thawing in liquid nitrogen, incubation for 20 min at 25 °C and adding the sarcosyl to final concentration 0.5%. The samples were then centrifuged at 40,000 x g for 90 min at 4 °C, the pellet was resuspended in ice-cold 10 mM Tris-HCl (pH 8.0) and frozen in liquid nitrogen. Gradient enriched EVs were isolated as above described (Fig. S1C). For proteomics, the samples were denatured by addition of 1 x SDS loading buffer. In-gel trypsin digestion was performed according to standard procedures (Shevchenko *et al.*, 2006). Briefly, 2 µg of EV and OM samples and 20 µg of WC samples were loaded on a NuPAGE 4-12% Bis-Tris Protein gels (Thermofisher Scientific, US), and the gels were run for 3 min only. Subsequently, the still not size-separated single protein band per sample was cut, reduced (50 mM DTT), alkylated (55 mm CAA, chloroacetamid) and digested overnight with trypsin (trypsin-gold, Promega).

LC-MS/MS data acquisition

Peptides generated by in-gel trypsin digestion were dried in a vacuum concentrator and dissolved in 0.1% formic acid (FA). LC-MS/MS measurements were performed on a Fusion Lumos Tribrid mass spectrometer (Thermo Fisher Scientific) equipped with an Ultimate 3000 RSLCnano system. Peptides were delivered to a trap column (ReproSil-pur C18-AQ, 5 µm, Dr Maisch, 20 mm × 75 µm, self-packed) at a flow rate of 5 µL/min in 100% solvent A (0.1% formic acid in HPLC grade water). After 10 min of loading, peptides were transferred to an

706 analytical column (ReproSil Gold C18-AQ, 3 µm, Dr Maisch, 400 mm × 75 µm, self-packed)
707 and separated using a 50 min gradient from 4% to 32% of solvent B (0.1% formic acid in
708 acetonitrile and 5% (v/v) DMSO) at 300 nL/min flow rate. Both nanoLC solvents contained 5%
709 (v/v) DMSO.

710

711 The Fusion Lumos Tribrid mass spectrometer was operated in data dependent acquisition and
712 positive ionization mode. MS1 spectra (360–1300 m/z) were recorded at a resolution of 60,000
713 using an automatic gain control (AGC) target value of 4e5 and maximum injection time
714 (maxIT) of 50 ms. After peptide fragmentation using higher energy collision induced
715 dissociation (HCD), MS2 spectra of up to 20 precursor peptides were acquired at a resolution
716 of 15.000 with an automatic gain control (AGC) target value of 5e4 and maximum injection
717 time (maxIT) of 22 ms. The precursor isolation window width was set to 1.3 m/z and normalized
718 collision energy to 30%. Dynamic exclusion was enabled with 20 s exclusion time (mass
719 tolerance +/-10 ppm).

720

721 **Computational analysis of proteomes**

722 LFQ values were used in the statistical analysis of proteome data. To select EV-enriched
723 proteins, Welch t-test were used to compare protein intensities between EV and WC samples.
724 The resulted p-values were corrected using the Benjamini-Hochberg method to control the false
725 discovery rate (FDR). The proteins with FDR < 0.05 and with the intensity in EV at least twice
726 higher than in WC were selected as EV-enriched proteins (n = 207). In addition, we selected
727 proteins that were exclusively identified in at least three (out of four) replicates of EV. (n =
728 162). A complete list of EV-enriched proteins is given in Table S1. The functional enrichment
729 analysis of the EV proteins were performed using the DAVID functional annotation tool (Huang

730 da *et al.*, 2009a, Huang da *et al.*, 2009b).

731

732 **Database searches**

733 Peptide identification and quantification was performed using MaxQuant (version 1.6.3.4) with
734 its built-in search engine Andromeda (Cox *et al.*, 2011, Tyanova *et al.*, 2016). MS2 spectra
735 were searched against a *Pseudomonas syringae pv tomato* protein database (UP000002515,
736 downloaded from Uniprot 04.05.2020) supplemented with common contaminants (built-in
737 option in MaxQuant). For all MaxQuant searches default parameters were employed. Those
738 included carbamidomethylation of cysteine as fixed modification and oxidation of methionine
739 and N-terminal protein acetylation as variable modifications. Trypsin/P was specified as
740 proteolytic enzyme. Precursor tolerance was set to 4.5 ppm, and fragment ion tolerance to 20
741 ppm. Results were adjusted to 1% false discovery rate (FDR) on peptide spectrum match (PSM)
742 and protein level, employing a target-decoy approach using reversed protein sequences. Label-
743 free quantification (LFQ algorithm) was enabled. The minimal peptide length was defined as 7
744 amino acids and the "match-between-run" function was not enabled. Each sample type (EV,
745 OM, WC) was analysed in biological quadruplicates (Table S1).

746

747 We used available localization prediction data at pseudomonas genome database
748 (pseudomonas.com) (Winsor *et al.*, 2016). Predicted protein localizations are presented as
749 stacked bar charts (made in MS Excel) as percentage to total number of the proteins in analyzed
750 sample. We used the available software DAVID bioinformatic resource 6.8
751 (https://david.ncifcrf.gov/) for GO term and KEGG pathway analysis, and the adjusted p-value
752 cut-off was set to 0.05 (Huang da *et al.*, 2009a, Huang da *et al.*, 2009b). We compared the EV
753 enriched proteins from *Pto* DC3000 with EV proteomes from planktonic grown *P. aeruginosa*
754 PAO1 (Choi *et al.*, 2011, Park *et al.*, 2014, Reales-Calderon *et al.*, 2015). We focussed on the

proteins that were identified in OMVs from *P. aeruginosa* PAO1 across all three studies and identified their gene orthologs in *Pto* DC3000 using the pseudomonas genome database (pseudomonas.com) (Winsor *et al.*, 2016). This set of proteins was compared to the *Pto* DC3000 EV-enriched proteins to predict EV biomarkers. The EV-enriched proteins were also compared with available *in planta Pto* DC3000 transcriptome and proteome data (Nobori *et al.*, 2018) (Nobori *et al.*, 2020).

Immunoblot analysis

Standard immunoblot analysis was performed according to Sambrook at al. (1989). 10% SDS-PAGE gels were blotted onto PVDF Immobilon-P membranes (Millipore). *Pto* DC3000 OprF was detected using 1:2,000 diluted rabbit polyclonal antibody against OprF from *Pseudomonas aeruginosa* (Cusabio Biotech Co.). As secondary antibody, we used a 1:50,000 dilution of the anti-rabbit IgG-Peroxidase polyclonal antibody (Sigma-Aldrich, A0545). Signal detection was done using SuperSignal West FemtoMaximum Sensitivity Substrate (Pierce, Thermo Scientific), according to manufacturer's instructions, and the images were captured using Vilber Lourmat Peqlab FUSION SL Gel Chemiluminescence Documentation System.

Statistical analysis

Student *t*-test, Welsch´s *t*-test, One-way ANOVA followed by Tukey multiple comparisons test and Welsch´s ANOVA with Dunnett´s T3 multiple comparisons post hoc test were performed using GraphPad Prism version 8.3 for Windows, GraphPad Software, San Diego, California USA, www.graphpad.com

Data availability

The mass spectrometry proteomics data have been deposited to the ProteomeXchange

Consortium via the PRIDE (Perez-Riverol *et al.*, 2019) partner repository with the dataset identifier PXD023971.

Author contributions

M.J. and S.R. designed research; M.J., C.L., K.R., C.M., L.B., B.S., A.B., A.K. performed research; M.J., C.L., K.R., C.M., A.B., A.K. and S.R. analysed data; E.S., J.S., F.M., J.M. developed protocols; M.J. and S.R. wrote the paper with inputs from all authors.

Acknowledgements

We like to thank members of the Robatzek laboratory for fruitful discussions. We acknowledge Lucia Grenga and Catriona Thompson (JIC), Franziska Hackbarth and Hermine Kienberger (BayBioMS) for their laboratory assistance, Miriam Abele for her mass spectrometric support at the BayBioMS as well as Jennifer Grünert and Cornelia Niemann (LMU Biocenter) for technical assistance in electron microscopy. This research was supported by the Deutsche Forschungsgemeinschaft (to S.R.) through a Heisenberg fellowship (RO 3550/14-1) and the SFB924 “Yield” (TP B15). M.J. was supported by the European Structural and Investment Funds, OP RDE-funded project ‘CHEMFELLS4UCTP’ (no. CZ.02.2.69/0.0/0.0/17_050/0008485).

Supplemental Information

Figure S1. A) The full-size SEM micrograph used in Fig. 1A of *Pto* DC3000 growth in planktonic culture (OD_{600} = 3-4). **B)** Size profile of EVs from *Pto* DC3000 planktonic cultures in fluid samples (OD_{600} = 7.5-11).

Figure S2. Isolation of *Pto* DC3000 EVs. A) Schematic overview of EVs isolation from planktonic cultures for fluid sample (1) and gradient enriched sample (2) analysis. **B)** Growth measurements of planktonic *Pto* DC3000 cultures. Orange indicates EV isolation from early exponential growth stages (OD_{600} = 1-2); green indicates EV isolation from late exponential growth stages (OD_{600} = 3-4). **C)** Schematic overview of EVs isolation from biofilm cultures. **D)** Growth measurements of biofilm *Pto* DC3000 cultures. The green dot represents the growth stage from which the bacteria were used for experiments.

Figure S3. Biophysical parameters of particles in apoplastic fluids from *A. thaliana* plants infected with *Pto* DC3000. A, D, G) Particle parameters over days post infection (dpi). **B, E, H)** Particle parameters in response to inoculation with different *Pto* DC3000 densities. **C, F, I)** Particle parameters in response to inoculation with different *Pto* DC3000 and co-treatment with flg22. Each dot represents value of independent samples for size and ζ-potential it represents median. 3-12 independent samples were used for each experiment. **J, K)** The profile of ζ-potential for each particle collected from apoplastic fluids of plants treated as indicated and gradient enriched EVs. Control = 0.2 mM EDTA; flg22 = 100 nM; n.t. = not treated; *Pto* DC3000 OD_{600} = 0.0006. Each treatment was 3 days long. The dots represent the mean across the ζ-potential values from independent samples: n = 8 (control); n = 10 (*Pto* DC3000); n = 6 (flg22); n = 4 (non-treatment).

824 **Figure S4. Pre-treatment with *Pto* DC3000 EVs induces resistance against subsequent *Pto***
825 **DC3000 infection. A)** Three individual biological repeats of *Pto* DC3000 growth (CFU) after
826 infection into leaves of *A. thaliana* without and with EV pre-treatment at 3 dpi (control = 0.02
827 mM EDTA). Each biological repeat consists of 12 independent samples. **B)** *Pto* DC3000 growth
828 (CFU) after infection (3 dpi) into leaves of *A. thaliana* without and with 100 nM flg22 1 day
829 pre-treatment (mock = 10 mM $MgCl_2$) n = 4. Asterisks represent the statistical difference
830 between the treated and control samples (two tailed Student t-test $p < 0.01$).
831
832 **Figure S5. Characteristics of the proteomic analysis. A)** Barplot shows the number of
833 identified proteins in each replicate. The solid line indicates the cumulative protein IDs and
834 dashed line shows the shared protein IDs. **B)** Boxplot shows a comparable distribution of
835 protein intensities from each replicate.
836
837 **Figure S6. Biophysical parameters of *Pto* DC3000 EVs across isolation methods. A-C)**
838 NTA measurements of particle concentration (A), ζ-potential (B) and size (C) of *Pto* DC3000
839 EVs collected from each step of gradient enrichment. **D-E)** NTA analysis of particle ζ-potential
840 (D) and size (E) of *Pto* DC3000 EVs from fluid samples before (live) and after boiling. Each
841 dot represents an independent sample.
842
843 **Table S1.** Filtered proteomics data with proteins that were identified in at least in three out of
844 four biological repeats in at least one variant (WC, OM and EV). Values used for volcano plot:
845 Highlighted EV-enriched proteins. Subcellar localization of identified proteins. Flagellar
846 proteins identified in EV enriched proteins.
847
848 **Table S2.** GO analysis of EV-enriched proteins

849

850 **Table S3.** Expression of EV-enriched proteins *in planta*

851

852 **Table S4.** *Pseudomonas* EV "core"

853

References

Alves NJ, Turner KB, Medintz IL, Walper SA. 2016. Protecting enzymatic function through directed packaging into bacterial outer membrane vesicles. *Sci Rep* **6**: 24866

Andriankaja A, Boisson-Dernier A, Frances L, Sauviac L, Jauneau A, Barker DG, de Carvalho-Niebel F. 2007. AP2-ERF transcription factors mediate Nod factor dependent Mt ENOD11 activation in root hairs via a novel cis-regulatory motif. *Plant Cell* **19**: 2866-85

Arigita C, Jiskoot W, Westdijk J, van Ingen C, Hennink WE, Crommelin DJ, Kersten GF. 2004. Stability of mono- and trivalent meningococcal outer membrane vesicle vaccines. *Vaccine* **22**: 629-42

Ashburner M, Ball CA, Blake JA, Botstein D, Butler H, Cherry JM, Davis AP, Dolinski K, Dwight SS, Eppig JT, Harris MA, Hill DP, Issel-Tarver L, Kasarskis A, Lewis S, Matese JC, Richardson JE, Ringwald M, Rubin GM, Sherlock G. 2000. Gene ontology: tool for the unification of biology. The Gene Ontology Consortium. *Nat Genet* **25**: 25-9

Bahar O, Mordukhovich G, Luu DD, Schwessinger B, Daudi A, Jehle AK, Felix G, Ronald PC. 2016. Bacterial Outer Membrane Vesicles Induce Plant Immune Responses. *Molecular Plant-Microbe Interactions* **29**: 374-384

Bachurski D, Schuldner M, Nguyen PH, Malz A, Reiners KS, Grenzi PC, Babatz F, Schauss AC, Hansen HP, Hallek M, von Strandmann EP. 2019. Extracellular vesicle measurements with nanoparticle tracking analysis - An accuracy and repeatability comparison between NanoSight NS300 and ZetaView. *Journal of Extracellular Vesicles* **8**

Bauman SJ, Kuehn MJ. 2006. Purification of outer membrane vesicles from Pseudomonas aeruginosa and their activation of an IL-8 response. *Microbes Infect* **8**: 2400-8

Bielska E, Birch PRJ, Buck AH, Abreu-Goodger C, Innes RW, Jin H, Pfaffl MW, Robatzek S, Regev-Rudzki N, Tisserant C, Wang S, Weiberg A. 2019. Highlights of the mini-symposium on extracellular vesicles in inter-organismal communication, held in Munich, Germany, August 2018. *Journal of Extracellular Vesicles* **8**: 1590116

Block A, Alfano JR. 2011. Plant targets for Pseudomonas syringae type III effectors: virulence targets or guarded decoys? *Curr Opin Microbiol* **14**: 39-46

Bredow M, Sementchoukova I, Siegel K, Monaghan J. 2019. Pattern-Triggered Oxidative Burst and Seedling Growth Inhibition Assays in Arabidopsis thaliana. *J Vis Exp*

Buttner D, Bonas U. 2010. Regulation and secretion of Xanthomonas virulence factors. *FEMS Microbiol Rev* **34**: 107-33

Campos ML, de Souza CM, de Oliveira KBS, Dias SC, Franco OL. 2018. The role of antimicrobial peptides in plant immunity. *J Exp Bot* **69**: 4997-5011

Couto D, Zipfel C. 2016. Regulation of pattern recognition receptor signalling in plants. *Nature Reviews Immunology* **16**: 537-52

Couto N, Schooling SR, Dutcher JR, Barber J. 2015. Proteome Profiles of Outer Membrane Vesicles and Extracellular Matrix of Pseudomonas aeruginosa Biofilms. *J Proteome Res* **14**: 4207-22

Cox J, Neuhauser N, Michalski A, Scheltema RA, Olsen JV, Mann M. 2011. Andromeda: a peptide search engine integrated into the MaxQuant environment. *Journal of Proteome Research* **10**: 1794-805

Czechowski T, Stitt M, Altmann T, Udvardi MK, Scheible WR. 2005. Genome-wide identification and testing of superior reference genes for transcript normalization in Arabidopsis. *Plant Physiol* **139**: 5-17

Devos S, Van Oudenhove L, Stremersch S, Van Putte W, De Rycke R, Van Driessche G, Vitse J, Raemdonck K, Devreese B. 2015. The effect of imipenem and diffusible signaling

902 factors on the secretion of outer membrane vesicles and associated Ax21 proteins in
903 Stenotrophomonas maltophilia. *Front Microbiol* **6**: 298
904 **Devos S, Van Putte W, Vitse J, Van Driessche G, Stremersch S, Van Den Broek W,**
905 **Raemdonck K, Braeckmans K, Stahlberg H, Kudryashev M, Savvides SN, Devreese B.**
906 2017. Membrane vesicle secretion and prophage induction in multidrug-resistant
907 Stenotrophomonas maltophilia in response to ciprofloxacin stress. *Environ Microbiol* **19**:
908 3930-3937
909 **Dodds PN, Rathjen JP.** 2010. Plant immunity: towards an integrated view of plant-
910 pathogen interactions. *Nat Rev Genet* **11**: 539-48
911 **Feitosa-Junior OR, Stefanello E, Zaini PA, Nascimento R, Pierry PM, Dandekar AM,**
912 **Lindow SE, da Silva AM.** 2019. Proteomic and Metabolomic Analyses of Xylella fastidiosa
913 OMV-Enriched Fractions Reveal Association with Virulence Factors and Signaling
914 Molecules of the DSF Family. *Phytopathology* **109**: 1344-1353
915 **Figaj D, Ambroziak P, Przepiora T, Skorko-Glonek J.** 2019. The Role of Proteases in the
916 Virulence of Plant Pathogenic Bacteria. *Int J Mol Sci* **20**
917 **Flechsler J, Heimerl T, Pickl C, Rachel R, Stierhof YD, Klingl A.** 2020. 2D and 3D
918 immunogold localization on (epoxy) ultrathin sections with and without osmium
919 tetroxide. *Microsc Res Tech* **83**: 691-705
920 **Frank J, Richter M, de Rossi C, Lehr CM, Fuhrmann K, Fuhrmann G.** 2018. Extracellular
921 vesicles protect glucuronidase model enzymes during freeze-drying. *Sci Rep* **8**: 12377
922 **Hall BM, Breidenstein EBM, de la Fuente-Nunez C, Reffuveille F, Mawla GD, Hancock**
923 **REW, Baker TA.** 2017. Two Isoforms of Clp Peptidase in Pseudomonas aeruginosa
924 Control Distinct Aspects of Cellular Physiology. *Journal of Bacteriology* **199**
925 **Huang da W, Sherman BT, Lempicki RA.** 2009a. Bioinformatics enrichment tools: paths
926 toward the comprehensive functional analysis of large gene lists. *Nucleic Acids Res* **37**: 1-
927 13
928 **Huang da W, Sherman BT, Lempicki RA.** 2009b. Systematic and integrative analysis of
929 large gene lists using DAVID bioinformatics resources. *Nature Protocols* **4**: 44-57
930 **Choi DS, Kim DK, Choi SJ, Lee J, Choi JP, Rho S, Park SH, Kim YK, Hwang D, Gho YS.**
931 2011. Proteomic analysis of outer membrane vesicles derived from Pseudomonas
932 aeruginosa. *Proteomics* **11**: 3424-9
933 **Chowdhury C, Jagannadham MV.** 2013. Virulence factors are released in association
934 with outer membrane vesicles of Pseudomonas syringae pv. tomato T1 during normal
935 growth. *Biochim Biophys Acta* **1834**: 231-9
936 **Ionescu M, Zaini PA, Baccari C, Tran S, da Silva AM, Lindow SE.** 2014. Xylella fastidiosa
937 outer membrane vesicles modulate plant colonization by blocking attachment to surfaces.
938 *Proceedings of the National Academy of Sciences of the United States of America* **111**:
939 E3910-E3918
940 **Kanehisa M, Goto S, Furumichi M, Tanabe M, Hirakawa M.** 2010. KEGG for
941 representation and analysis of molecular networks involving diseases and drugs. *Nucleic*
942 *Acids Res* **38**: D355-60
943 **Kaparakis-Liaskos M, Ferrero RL.** 2015. Immune modulation by bacterial outer
944 membrane vesicles. *Nature Reviews Immunology* **15**: 375-387
945 **Klimentova J, Stulik J.** 2015. Methods of isolation and purification of outer membrane
946 vesicles from gram-negative bacteria. *Microbiol Res* **170**: 1-9
947 **Knoke LR, Abad Herrera S, Gotz K, Justesen BH, Gunther Pomorski T, Fritz C,**
948 **Schakermann S, Bandow JE, Aktas M.** 2020. Agrobacterium tumefaciens Small
949 Lipoprotein Atu8019 Is Involved in Selective Outer Membrane Vesicle (OMV) Docking to
950 Bacterial Cells. *Front Microbiol* **11**: 1228

Krckova Z, Kocourkova D, Danek M, Brouzdova J, Pejchar P, Janda M, Pokotylo I, Ott PG, Valentova O, Martinec J. 2018. The Arabidopsis thaliana non-specific phospholipase C2 is involved in the response to Pseudomonas syringae attack. *Annals of Botany* **121**: 297-310

Kunze G, Zipfel C, Robatzek S, Niehaus K, Boller T, Felix G. 2004. The N terminus of bacterial elongation factor Tu elicits innate immunity in Arabidopsis plants. *Plant Cell* **16**: 3496-3507

Kvitko BH, Park DH, Velasquez AC, Wei CF, Russell AB, Martin GB, Schneider DJ, Collmer A. 2009. Deletions in the repertoire of Pseudomonas syringae pv. tomato DC3000 type III secretion effector genes reveal functional overlap among effectors. *Plos Pathogens* **5**: e1000388

Lappann M, Otto A, Becher D, Vogel U. 2013. Comparative proteome analysis of spontaneous outer membrane vesicles and purified outer membranes of Neisseria meningitidis. *Journal of Bacteriology* **195**: 4425-35

Lovelace AH, Smith A, Kvitko BH. 2018. Pattern-Triggered Immunity Alters the Transcriptional Regulation of Virulence-Associated Genes and Induces the Sulfur Starvation Response in Pseudomonas syringae pv. tomato DC3000. *Mol Plant Microbe Interact* **31**: 750-765

Macdonald IA, Kuehn MJ. 2013. Stress-induced outer membrane vesicle production by Pseudomonas aeruginosa. *Journal of Bacteriology* **195**: 2971-81

Manabe T, Kato M, Ueno T, Kawasaki K. 2013. Flagella proteins contribute to the production of outer membrane vesicles from Escherichia coli W3110. *Biochem Biophys Res Commun* **441**: 151-6

Mansfield J, Genin S, Magori S, Citovsky V, Sriariyanum M, Ronald P, Dow M, Verdier V, Beer SV, Machado MA, Toth I, Salmond G, Foster GD. 2012. Top 10 plant pathogenic bacteria in molecular plant pathology. *Molecular Plant Pathology* **13**: 614-629

McBroom AJ, Johnson AP, Vemulapalli S, Kuehn MJ. 2006. Outer membrane vesicle production by Escherichia coli is independent of membrane instability. *Journal of Bacteriology* **188**: 5385-5392

McBroom AJ, Kuehn MJ. 2007. Release of outer membrane vesicles by Gram-negative bacteria is a novel envelope stress response. *Mol Microbiol* **63**: 545-58

McCaig WD, Koller A, Thanassi DG. 2013. Production of outer membrane vesicles and outer membrane tubes by Francisella novicida. *Journal of Bacteriology* **195**: 1120-32

McMillan HM, Zebell SG, Ristaino JB, Dong X, Kuehn MJ. 2020. Protective Plant Immune Responses are Elicited by Bacterial Outer Membrane Vesicles. *BioRxiv*

Melotto M, Underwood W, Koczan J, Nomura K, He SY. 2006. Plant stomata function in innate immunity against bacterial invasion. *Cell* **126**: 969-80

Mersmann S, Bourdais G, Rietz S, Robatzek S. 2010. Ethylene signaling regulates accumulation of the FLS2 receptor and is required for the oxidative burst contributing to plant immunity. *Plant Physiology* **154**: 391-400

Metruccio MM, Evans DJ, Gabriel MM, Kadurugamuwa JL, Fleiszig SM. 2016. Pseudomonas aeruginosa Outer Membrane Vesicles Triggered by Human Mucosal Fluid and Lysozyme Can Prime Host Tissue Surfaces for Bacterial Adhesion. *Front Microbiol* **7**: 871

Nascimento R, Gouran H, Chakraborty S, Gillespie HW, Almeida-Souza HO, Tu A, Rao BJ, Feldstein PA, Bruening G, Goulart LR, Dandekar AM. 2016. The Type II Secreted Lipase/Esterase LesA is a Key Virulence Factor Required for Xylella fastidiosa Pathogenesis in Grapevines. *Scientific Reports* **6**

Nobori T, Velasquez AC, Wu JN, Kvitko BH, Kremer JM, Wang Y, He SY, Tsuda K. 2018. Transcriptome landscape of a bacterial pathogen under plant immunity. *Proceedings of the National Academy of Sciences of the United States of America* **115**: E3055-E3064

Nobori T, Wang Y, Wu J, Stolze SC, Tsuda Y, Finkemeier I, Nakagami H, Tsuda K. 2020. Multidimensional gene regulatory landscape of a bacterial pathogen in plants. *Nat Plants*

Nobori T, Yiming W, Jingni W, Christina SS, Yayoi T, Iris F, Hirofumi N, Kenichi T. 2019. In planta bacterial multi-omics analysis illuminates regulatory principles underlying plant-pathogen interactions. *BioRxiv*

Nomura K, Debroy S, Lee YH, Pumplin N, Jones J, He SY. 2006. A bacterial virulence protein suppresses host innate immunity to cause plant disease. *Science* **313**: 220-3

Park AJ, Murphy K, Krieger JR, Brewer D, Taylor P, Habash M, Khursigara CM. 2014. A temporal examination of the planktonic and biofilm proteome of whole cell Pseudomonas aeruginosa PAO1 using quantitative mass spectrometry. *Mol Cell Proteomics* **13**: 1095-105

Perez-Cruz C, Delgado L, Lopez-Iglesias C, Mercade E. 2015. Outer-inner membrane vesicles naturally secreted by gram-negative pathogenic bacteria. *Plos One* **10**: e0116896

Perez-Riverol Y, Csordas A, Bai J, Bernal-Llinares M, Hewapathirana S, Kundu DJ, Inuganti A, Griss J, Mayer G, Eisenacher M, Perez E, Uszkoreit J, Pfeuffer J, Sachsenberg T, Yilmaz S, Tiwary S, Cox J, Audain E, Walzer M, Jarnuczak AF *et al.* 2019. The PRIDE database and related tools and resources in 2019: improving support for quantification data. *Nucleic Acids Res* **47**: D442-D450

Prados-Rosales R, Weinrick BC, Pique DG, Jacobs WR, Jr., Casadevall A, Rodriguez GM. 2014. Role for Mycobacterium tuberculosis membrane vesicles in iron acquisition. *Journal of Bacteriology* **196**: 1250-6

Raposo G, Stoorvogel W. 2013. Extracellular vesicles: exosomes, microvesicles, and friends. *J Cell Biol* **200**: 373-83

Reales-Calderon JA, Corona F, Monteoliva L, Gil C, Martinez JL. 2015. Quantitative proteomics unravels that the post-transcriptional regulator Crc modulates the generation of vesicles and secreted virulence determinants of Pseudomonas aeruginosa. *Data Brief* **4**: 450-3

Roier S, Zingl FG, Cakar F, Durakovic S, Kohl P, Eichmann TO, Klug L, Gadermaier B, Weinzerl K, Prassl R, Lass A, Daum G, Reidl J, Feldman MF, Schild S. 2016. A novel mechanism for the biogenesis of outer membrane vesicles in Gram-negative bacteria. *Nature Communications* **7**: 10515

Rossbach S, Wilson TL, Kukuk ML, Carty HA. 2000. Elevated zinc induces siderophore biosynthesis genes and a zntA-like gene in Pseudomonas fluorescens. *FEMS Microbiol Lett* **191**: 61-70

Roszkowiak J, Jajor P, Gula G, Gubernator J, Zak A, Drulis-Kawa Z, Augustyniak D. 2019. Interspecies Outer Membrane Vesicles (OMVs) Modulate the Sensitivity of Pathogenic Bacteria and Pathogenic Yeasts to Cationic Peptides and Serum Complement. *Int J Mol Sci* **20**

Rutter BD, Innes RW. 2017. Extracellular Vesicles Isolated from the Leaf Apoplast Carry Stress-Response Proteins. *Plant Physiology* **173**: 728-741

Rybak K, Robatzek S. 2019. Functions of Extracellular Vesicles in Immunity and Virulence. *Plant Physiology* **179**: 1236-1247

Sampath V, McCaig WD, Thanassi DG. 2018. Amino acid deprivation and central carbon metabolism regulate the production of outer membrane vesicles and tubes by Francisella. *Mol Microbiol* **107**: 523-541

Shevchenko A, Tomas H, Havlis J, Olsen JV, Mann M. 2006. In-gel digestion for mass spectrometric characterization of proteins and proteomes. *Nat Protoc* **1**: 2856-60

Schechter LM, Vencato M, Jordan KL, Schneider SE, Schneider DJ, Collmer A. 2006. Multiple approaches to a complete inventory of Pseudomonas syringae pv. tomato DC3000 type III secretion system effector proteins. *Mol Plant Microbe Interact* **19**: 1180-92

Schindelin J, Arganda-Carreras I, Frise E, Kaynig V, Longair M, Pietzsch T, Preibisch S, Rueden C, Saalfeld S, Schmid B, Tinevez JY, White DJ, Hartenstein V, Eliceiri K, Tomancak P, Cardona A. 2012. Fiji: an open-source platform for biological-image analysis. *Nat Methods* **9**: 676-82

Schwechheimer C, Kuehn MJ. 2015. Outer-membrane vesicles from Gram-negative bacteria: biogenesis and functions. *Nature Reviews Microbiology* **13**: 605-619

Sidhu VK, Vorholter FJ, Niehaus K, Watt SA. 2008. Analysis of outer membrane vesicle associated proteins isolated from the plant pathogenic bacterium Xanthomonas campestris pv. campestris. *Bmc Microbiology* **8**

Sole M, Scheibner F, Hoffmeister AK, Hartmann N, Hause G, Rother A, Jordan M, Lautier M, Arlat M, Buttner D. 2015. Xanthomonas campestris pv. vesicatoria Secretes Proteases and Xylanases via the Xps Type II Secretion System and Outer Membrane Vesicles. *Journal of Bacteriology* **197**: 2879-2893

The Gene Ontology C. 2019. The Gene Ontology Resource: 20 years and still GOing strong. *Nucleic Acids Res* **47**: D330-D338

Toyofuku M, Nomura N, Eberl L. 2019. Types and origins of bacterial membrane vesicles. *Nature Reviews Microbiology* **17**: 13-24

Turnbull L, Toyofuku M, Hynen AL, Kurosawa M, Pessi G, Petty NK, Osvath SR, Carcamo-Oyarce G, Gloag ES, Shimoni R, Omasits U, Ito S, Yap X, Monahan LG, Cavaliere R, Ahrens CH, Charles IG, Nomura N, Eberl L, Whitchurch CB. 2016. Explosive cell lysis as a mechanism for the biogenesis of bacterial membrane vesicles and biofilms. *Nature Communications* **7**: 11220

Tyanova S, Temu T, Cox J. 2016. The MaxQuant computational platform for mass spectrometry-based shotgun proteomics. *Nat Protoc* **11**: 2301-2319

Vinatzer BA, Teitzel GM, Lee MW, Jelenska J, Hotton S, Fairfax K, Jenrette J, Greenberg JT. 2006. The type III effector repertoire of Pseudomonas syringae pv. syringae B728a and its role in survival and disease on host and non-host plants. *Mol Microbiol* **62**: 26-44

Wan WL, Frohlich K, Pruitt RN, Nurnberger T, Zhang L. 2019. Plant cell surface immune receptor complex signaling. *Current Opinion in Plant Biology* **50**: 18-28

Wang Y, Garrido-Oter R, Wu J, Winkelmuller TM, Agler M, Colby T, Nobori T, Kemen E, Tsuda K. 2019. Site-specific cleavage of bacterial MucD by secreted proteases mediates antibacterial resistance in Arabidopsis. *Nature Communications* **10**: 2853

Wei HL, Zhang W, Collmer A. 2018. Modular Study of the Type III Effector Repertoire in Pseudomonas syringae pv. tomato DC3000 Reveals a Matrix of Effector Interplay in Pathogenesis. *Cell Rep* **23**: 1630-1638

Wilson M, Campbell HL, Ji P, Jones JB, Cuppels DA. 2002. Biological control of bacterial speck of tomato under field conditions at several locations in north america. *Phytopathology* **92**: 1284-92

Winsor GL, Griffiths EJ, Lo R, Dhillon BK, Shay JA, Brinkman FS. 2016. Enhanced annotations and features for comparing thousands of Pseudomonas genomes in the Pseudomonas genome database. *Nucleic Acids Res* **44**: D646-53

Xin XF, He SY. 2013. Pseudomonas syringae pv. tomato DC3000: a model pathogen for probing disease susceptibility and hormone signaling in plants. *Annu Rev Phytopathol* **51**: 473-98

Xin XF, Kvitko B, He SY. 2018. Pseudomonas syringae: what it takes to be a pathogen. *Nature Reviews Microbiology* **16**: 316-328

Zingl FG, Kohl P, Cakar F, Leitner DR, Mitterer F, Bonnington KE, Rechberger GN, Kuehn MJ, Guan Z, Reidl J, Schild S. 2020. Outer Membrane Vesiculation Facilitates Surface Exchange and In Vivo Adaptation of Vibrio cholerae. *Cell Host & Microbe* **27**: 225-237 e8

Zipfel C, Kunze G, Chinchilla D, Caniard A, Jones JD, Boller T, Felix G. 2006. Perception of the bacterial PAMP EF-Tu by the receptor EFR restricts Agrobacterium-mediated transformation. *Cell* **125**: 749-60

Zipfel C, Robatzek S, Navarro L, Oakeley EJ, Jones JD, Felix G, Boller T. 2004. Bacterial disease resistance in Arabidopsis through flagellin perception. *Nature* **428**: 764-7